Title

A multifunctional Wnt regulator underlies the evolution of rodent stripe patterns

Journal

Nature Ecology & Evolution, 7(12)

ISSN

2397-334X

Authors

Johnson, Matthew R

Li, Sha

Guerrero-Juarez, Christian F

et al.

Publication Date

2023-12-01

DOI

10.1038/s41559-023-02213-7

Peer reviewed

HHS Public Access

Author manuscript

Nat Ecol Evol. Author manuscript; available in PMC 2024 February 05.

Published in final edited form as:

Nat Ecol Evol. 2023 December ; 7(12): 2143–2159. doi:10.1038/s41559-023-02213-7.

A multifunctional Wnt regulator underlies the evolution of rodent stripe patterns

Matthew R. Johnson[1,10], **Sha Li**[1,10], **Christian F. Guerrero-Juarez**[2,3,4,5,6], **Pearson Miller**[7], **Benjamin J. Brack**[1], **Sarah A. Mereby**[1], **Jorge A. Moreno**[1], **Charles Y. Feigin**[1], **Jenna Gaska**[1], **Jaime A. Rivera-Perez**[8], **Qing Nie**[3,4,5,6], **Alexander Ploss**[1], **Stanislav Y. Shvartsman**[1,7,9], **Ricardo Mallarino**[1]

[1]Department of Molecular Biology, Princeton University, Princeton, NJ, USA.

[2]Carle Illinois College of Medicine, University of Illinois at Urbana-Champaign, Urbana, IL, USA.

[3]Department of Developmental and Cell Biology, University of California, Irvine, CA, USA.

[4]Department of Mathematics, University of California, Irvine, CA, USA.

[5]Center for Complex Biological Systems, University of California, Irvine, CA, USA.

[6]NSF-Simons Center for Multiscale Cell Fate Research, University of California, Irvine, CA, USA.

[7]Center for Computational Biology, Flatiron Institute, New York, NY, USA.

[8]Frederick National Laboratory for Cancer Research, Frederick, MA, USA.

[9]The Lewis-Sigler Institute for Integrative Genomics, Princeton University, Princeton, NJ, USA.

[10]These authors contributed equally: Matthew R. Johnson, Sha Li.

Abstract

Animal pigment patterns are excellent models to elucidate mechanisms of biological organization. Although theoretical simulations, such as Turing reaction–diffusion systems, recapitulate many animal patterns, they are insufficient to account for those showing a high degree of spatial

Correspondence and requests for materials should be addressed to Ricardo Mallarino. rmallarino@princeton.edu.

Author contributions

M.R.J. and R.M. conceived the project and designed experiments. M.R.J. performed RNA-seq experiments and bulk RNA-seq analysis. S.L. performed the in vitro and in vivo genome editing in striped mice, with help from S.A.M. and J.A.R.-P. M.R.J. and S.L. performed all downstream processing and analysis of genome edited animals. P.M. and S.Y.S. did the mathematical modelling. C.F.G.-J. led the scRNA-seq analysis, with support from M.R.J. and Q.N. M.R.J., B.J.B. and R.M. performed in situ hybridizations. M.R.J., B.J.B., S.A.M. and R.M. performed the phenotypic characterization of striped mouse and laboratory mouse tissues, including immunofluorescence and histology. M.R.J. and S.A.M. performed the melanocyte cell culture experiments. J.A.M. did the evolutionary analysis. C.Y.F. generated the rhabdomyzed *Mus* genome and lift-over annotation. J.G. and A.P. generated the immortalized *Rhabdomys* fibroblasts. M.R.J. and R.M. wrote the manuscript with input from all authors.

Competing interests

The authors declare no competing interests.

Additional information

Extended data is available for this paper at https://doi.org/10.1038/s41559-023-02213-7.

Supplementary information The online version contains supplementary material available at https://doi.org/10.1038/s41559-023-02213-7.

Peer review information *Nature Ecology & Evolution* thanks Julien Debbache and Denis Headon for their contribution to the peer review of this work. Peer reviewer reports are available.

organization and reproducibility. Here, we study the coat of the African striped mouse (*Rhabdomys pumilio*) to uncover how periodic stripes form. Combining transcriptomics, mathematical modelling and mouse transgenics, we show that the Wnt modulator *Sfrp2* regulates the distribution of hair follicles and establishes an embryonic prepattern that foreshadows pigment stripes. Moreover, by developing in vivo gene editing in striped mice, we find that *Sfrp2* knockout is sufficient to alter the stripe pattern. Strikingly, mutants exhibited changes in pigmentation, revealing that *Sfrp2* also regulates hair colour. Lastly, through evolutionary analyses, we find that striped mice have evolved lineage-specific changes in regulatory elements surrounding *Sfrp2*, many of which may be implicated in modulating the expression of this gene. Altogether, our results show that a single factor controls coat pattern formation by acting both as an orienting signalling mechanism and a modulator of pigmentation. More broadly, our work provides insights into how spatial patterns are established in developing embryos and the mechanisms by which phenotypic novelty originates.

The skin of many vertebrate species displays characteristic periodic pigment patterns, such as spots and stripes, which play key roles in mediating intra- and inter-specific communication[1–4]. Because of their visual accessibility, extreme diversity and widespread occurrence among multiple species, colour patterns represent a fascinating model to understand the mechanisms underlying biological organization. While this research has been mostly restricted to a handful of traditional laboratory model species, recent advances in genomics and experimental approaches now offer the possibility of studying wild-derived species to uncover the processes that have generated the astonishing diversity of colour patterns found in nature.

Theoretical simulations involving Turing reaction–diffusion systems, in which activators and inhibitors interact to establish organized spatial patterns, can closely recapitulate a wide variety of periodic colour patterns seen in nature[5–7]. Notably, however, Turing-generated patterns are variable and sensitive to stochastic perturbation[8]. That is, Turing mechanisms are insufficient, by themselves, to explain the formation of periodic colour patterns seen in many species, which are characterized by a high degree of spatial organization and reproducibility across individuals[9–13]. Therefore, a long-standing challenge has been to uncover the molecular, cellular and developmental events by which periodic colour patterns are specified and organized.

The African striped mouse (*Rhabdomys pumilio*), a rodent that exhibits a naturally evolved coat pattern of dark and light parallel stripes (Fig. 1a), is a useful model in which to explore molecular mechanisms underlying periodic colour patterns because this mouse can be maintained and reared in the laboratory, allowing for controlled experiments and development of molecular tools[14]. Moreover, the African striped mouse and the laboratory mouse (*Mus musculus*), the premier model species in mammalian/skin research, are closely related[14], opening the door for powerful comparative studies. Here, we use a variety of multidisciplinary approaches to uncover the developmental mechanisms controlling coat pattern formation in striped mice.

Striped mice display regional variation in embryonic placode formation

Striped mice exhibit differences in hair length between striped skin regions that are apparent at early postnatal stages (Fig. 1b)[11]. We hypothesized that these differences may reflect stripe-specific alterations in the developmental timing of hair follicle placodes (hereafter referred to as placodes). In laboratory mice (*M. musculus*), placodes are visible at embryonic day 15.5 (E15.5) and are evenly distributed throughout the dorsal skin (Fig. 1c)[15,16]. Remarkably, this stereotyped spatial pattern differs considerably in striped mice. At the equivalent embryonic stage (that is, the emergence of visible placodes, around E16.5 in striped mice), whole-mount in situ hybridizations for early markers of placode formation (for example, *Dkk4, Ctnnb1, Wnt10b, Wif1* and *Dkk1*)[17] revealed that striped mouse dorsal placodes develop in a stripe-like, spatially restricted manner, whereby they are present in some regions along the dorsal skin but absent in others (Fig. 1c and Extended Data Fig. 1a,b). About 2 days later, at E18.5, placodes eventually become visible in regions previously devoid of them, as evidenced by thickening of the epidermis and the appearance of molecular markers (Extended Data Fig. 1c–e). Notably, stripe-like dorsal areas where placodes fail to form initially correspond to regions that will constitute the eventual dark pigment stripes, explaining why hair from dark stripes is shorter at birth and suggesting that spatially restricted patterns of embryonic placode formation foreshadow pigmentation stripes (Fig. 1d)[11].

Sfrp2 is expressed in a dorsoventral gradient during placode formation

To identify regulators of the striped mouse placode developmental pattern, we performed an unbiased bulk-level RNA-sequencing (RNA-seq) screen for genes differentially expressed between placode-rich and placode-barren skin regions in E16.5 embryos. We used the boundaries between these regions as a proxy to mark and isolate four distinct dorsal skin regions: R1 (the dorsal-most, placode-barren region), R2 (the dorsal-most, placode-rich region), R3 (the ventral-most, placode-barren region) and R4 (the ventral-most, placode-rich region) (Fig. 1e). Next, we did a series of pairwise comparisons (R1 versus R2; R1 versus R4; R2 versus R3; and R3 versus R4) to identify differentially expressed genes between placode-barren (R1 and R3) and placode-rich (R2 and R4) regions. Although each pairwise comparison yielded several differentially expressed genes (Fig. 1f and Supplementary Data 1), only one gene, the Wnt modulator *Sfrp2*, was differentially expressed in all four comparisons ($P_{adj} < 0.05$). Surprisingly, however, *Sfrp2* was neither upregulated nor downregulated in placode-barren (R1 and R3) or placode-rich regions (R2 and R4). Rather, this gene was always upregulated in the dorsal-most region among the two being compared (R1 > R2, R1 > R4, R2 > R3 and R3 > R4). Notably, in addition to *Sfrp2*, there were other Wnt modulators expressed in a dorsoventral gradient (*Dkk2*, *Igbf4*, *Rspo2* and *Rspo4*), although they were not always differentially expressed between the dorsal regions (Extended Data Fig. 2 and Supplementary Data 1).

Sfrp2 negatively regulates Wnt signalling in striped mouse embryonic skin

Since Wnt signals are required for the initiation of hair follicle development[17], *Sfrp2* constituted an attractive candidate for patterning striped mouse placodes. However, as

Sfrp2 can have dual roles as both an activator and repressor of Wnt signalling, depending on cellular microenvironment[18–21], the relationship between *Sfrp2* and Wnt signalling in striped mouse skin remained unclear. Moreover, whether *Sfrp2* plays a role in placode formation has not been previously investigated. To study this, we dissociated dorsal skin from regions R1, R2 and R3 of E16.5 embryos as before, and performed single-cell RNA-sequencing (scRNA-seq) on each of the regions. As described below, our experimental design allowed us to carry out complementary analyses, both in a combined pool of dorsal cells as well as in cells derived from the individual dorsal regions (R1–R3). First, we pooled an equal number of cells from R1–R3 and used established molecular markers[22–24] to identify the different cell types present. Our analysis identified 14 distinct cell types, all of which have been reported in laboratory mice from similar embryonic stages (Fig. 2a and Supplementary Table 1)[22–24]. Notably, analysis of 'placode keratinocyte' and 'dermal condensate' cell clusters revealed that placode-rich (R2) and placode-barren skin regions (R1 and R3) differed in the expression levels of most placode (for example, *Shh* and *Edar*)[25] and dermal condensate (for example, *Sox2*, *Alx4* and *Dkk1*)[26] markers (Extended Data Fig. 3). This result indicates that the macroscopic differences seen between R1 and R3 (Fig. 1c) are recapitulated at the molecular level. Among the different cell types identified in skin, *Sfrp2* was specifically expressed in dermal fibroblasts, primarily in those found in the reticular dermis (Fig. 2b and Extended Data Fig. 4a). In addition, comparisons among the different dorsal regions revealed that both the expression levels of *Sfrp2* in fibroblasts and the percentage of fibroblasts expressing *Sfrp2* were highest in R1 and lowest in R3 (Extended Data Fig. 4b), a result that is consistent with the dorsoventral expression gradient seen with our bulk RNA-seq data.

To uncover the mechanism of action of *Sfrp2* in the skin of striped mice, we next clustered fibroblasts based on *Sfrp2* expression to define a population of *Sfrp2*-high (>2 unique molecular identifiers (UMIs)) and *Sfrp2*-low (<2 UMIs) fibroblasts (Fig. 2c). Differential gene expression analysis between *Sfrp2*-high and *Sfrp2*-low cells yielded numerous genes ($P_{adj} < 0.05$), 482 of which were upregulated and 272 that were downregulated in *Sfrp2*-high compared to *Sfrp2*-low cells (Supplementary Data 2). Among the genes upregulated in *Sfrp2*-low fibroblasts, gene ontology analysis identified regulation of Wnt signalling as the most significantly enriched pathway (Fig. 2d). Indeed, expression of numerous Wnt-related genes, including key activators of the pathway (*Lef1* and *Ctnnb1*), were higher in *Sfrp2*-low (Fig. 2e and Supplementary Data 2) compared to *Sfrp2*-high cells, demonstrating that *Sfrp2* and Wnt activation are negatively correlated in striped mice dermal fibroblasts. To confirm and extend our previous observation, we examined spatial patterns of *Sfrp2* expression and Wnt signalling markers. RNA in situ hybridizations using hybridization chair reaction (HCR) in cross-sections from E16.5 striped mice embryos, coupled to immunofluorescence (IF) for an epidermal marker (KRT14), indicated that expression of *Sfrp2* was strong in mesenchymal cells directly above the neural tube and decreased laterally, a result consistent with our bulk-level RNA-seq analysis (Fig. 2f and Extended Data Fig. 5a). At this same stage, IF for CTNNB1 and LEF1 showed that these markers were readily detectable in epidermal cells from lateral and ventral regions of the embryo but were absent from cells above the neural tube and adjacent areas, where *Sfrp2* expression was highest (Fig. 2g and Extended Data Fig. 5b). This pattern contrasted with what was seen in stage-

matched laboratory mouse embryos (E15.5), which had overall lower levels of dermal *Sfrp2* expression (Fig. 2h) and uniform levels of LEF1 and CTNNB1 throughout the epidermis, including above the neural tube (Fig. 2i and Extended Data Fig. 5c).

Notably, the marked differences in *Sfrp2* expression between striped mouse and laboratory mouse were not only evident during placode formation but also in stages prior. Specifically, as indicated by scRNA-seq, the number of *Sfrp2*-expressing fibroblasts, as well as the average *Sfrp2* expression levels within those fibroblasts, steadily increased in the days preceding striped mouse placode emergence (E13.5–E16.5) (Fig. 2j). This pattern starkly contrasted with laboratory mouse, where *Sfrp2*-expressing fibroblasts initially rise (from E12.5 to E13.5) but then dramatically decrease (from E13.5 to E15.5). Moreover, average *Sfrp2* expression levels within laboratory mouse fibroblasts did not change throughout this period (Fig. 2k).

Taken together, our scRNA-seq data coupled to RNA in situ/IF analysis indicate that *Sfrp2* and Wnt signalling are negatively correlated, suggest that dermal *Sfrp2* expression acts to inhibit Wnt signalling, and indicate that the observed patterns are unique to striped mouse.

Sfrp2 overexpression alters placode formation in laboratory mouse

Wnt signalling is a primary determinant of hair follicle formation and spacing, as perturbation of members of this pathway leads to alterations in hair follicle number and distribution[16,17,27,28]. This raises the intriguing possibility that *Sfrp2* may be acting to directly regulate striped mouse placode development. If this is the case, one would predict that increasing expression of *Sfrp2* in embryonic skin with low endogenous levels of *Sfrp2*, such as that of laboratory mouse (Fig. 2h)[23,24], would alter placode formation. To test this, we generated $Rosa^{Sfrp2\text{-}GFP}$ mice, a strain that allowed us to activate *Sfrp2* transcription in the presence of a tissue-specific Cre driver. To establish whether dermal expression of *Sfrp2* was sufficient to alter placode formation, as implied by our striped mouse data, we crossed $Rosa^{Sfrp2\text{-}GFP}$ mice with *Dermo1-Cre* mice, which can be used to drive Cre expression in dermal fibroblasts[29,30], including those expressing *Sfrp2* (Extended Data Fig. 6). While this experiment is not designed to recapitulate the gradient-like expression of *Sfrp2* seen in striped mice, it allows us to test the functional effect of upregulating this gene exclusively in dermal fibroblasts. Double-transgenic embryos (*Dermo-Cre*;$Rosa^{Sfrp2\text{-}GFP}$) analysed at E17.5 showed a significant reduction in the number of placodes/hair follicles, compared to control littermates ($n = 4$) (Fig. 2l,m). Thus, our transgenic experiments in laboratory mice demonstrate a functional relationship between *Sfrp2* and embryonic placode development in which elevated levels of *Sfrp2* in the dermis lead to a marked reduction in the number of placodes/ hair follicles.

Modelling implicates *Sfrp2* in patterning striped mouse placodes

During striped mouse mid-embryogenesis, *Sfrp2* is expressed in a dorsoventral gradient and acts to negatively regulate Wnt signalling. Moreover, in line with its role as a Wnt inhibitor, *Sfrp2* caused a reduction in placode formation. The dorsoventral expression pattern of a placode inhibitor was, a priori, unexpected. However, previous work has pointed to upstream

morphogen gradients as a means for establishing stripe-like patterns[31]. In laboratory mouse, placode spacing is regulated by a self-organizing Turing reaction–diffusion system in which activators and inhibitors interact to establish an organized spatial pattern[32]. While the classic picture of stripe formation via a Turing instability features the emergence of patterns in response to global, spatially uniform perturbations, recent theoretical work has increasingly emphasized the capacity of spatial gradients to trigger the emergence of stripes[33]. We therefore turned to mathematical modelling to understand how a dorsoventral gradient could influence an underlying Turing pattern. Our approach was to start with a canonical set of equations for biochemical pattern formation, the Gierer–Meinhardt (GM) model[34], and separately, a simple model of a diffusible modulator with spatially non-uniform expression (Fig. 3a). As a modulator can be coupled to the GM system in various ways, we constructed a family of model variants which we studied in parallel (for example, in model 1, the modulator accelerates the local degradation of the activator; while in model 2, it interferes with the strength of the activator's positive feedback loop and so on) (Fig. 3b). Our analysis focused on two related phenomena: (1) the destabilization of the uniform steady state by the introduction of modulation and (2) the relationship between modulation and stripe spacing.

The bifurcation structure of GM is well-established in the absence of modulation, allowing us to choose a starting point in our parameter space featuring a stable uniform steady state and stable stripe patterns[35,36]. In other words, for our parameter choices, stripes will not spontaneously form from an initially uniform morphogen profile in response to noise or other small symmetry-breaking perturbations. However, spatial prepatterns can force pattern formation[33]. In this vein, we altered the parameter-controlling non-uniformity of modulator production, effectively tuning the gradient steepness while keeping total modulator production constant. In doing so, we found that for each of our model variants, a sufficiently strong gradient in modulator production would destabilize the uniform steady state and trigger pattern formation (Fig. 3c and Extended Data Fig. 7a,b). Thus, by altering the underlying Turing activity (changing it from uniform to non-uniform) a dorsoventral modulator may indeed explain differences between the absence (for example, laboratory mouse) or presence (for example, striped mouse) of stripes. We note that an alternative model based on positional information produces qualitatively different predictions (Extended Data Fig. 7c) that are not reflected in the experiments described below, supporting our suggestion that a Turing mechanism is the more likely candidate for patterning.

We next used additional simulations to study the relationship between alterations to the modulator gradient and potential consequences on stripe spacing. The results from our simulations demonstrated the continued stability of stripes, regardless of the magnitude of the modulator gradient (Extended Data Fig. 7b). More strikingly, however, we found that altering the strength of the modulator gradient led to stereotyped changes in the spacing of the stripes: in all models, changing only the magnitude of the modulator gradient produced subtle changes in stripe width (Fig. 3c,d and Extended Data Fig. 7b).

Taken together, our mathematical simulations coupled to our experimental data implicate *Sfrp2* as a key component of dorsoventral gradient that organizes placode patterns in

striped mouse. Furthermore, our simulations make testable predictions about the phenotypic changes that result from altering such a gradient.

In vivo gene editing in striped mice leads to changes in stripe width

To establish a direct causal link between *Sfrp2* and placode formation patterns as well as test the predictions from our mathematical simulations, it is critical to perform functional experiments directly in striped mice. To this end, we adapted a CRISPR-based experimental strategy in which recombinant adeno-associated viruses (rAAVs) are used to deliver CRISPR–Cas9 reagent into the oviduct of pregnant females. This in vivo gene editing technique is based on the ability of rAAV6 to pass through the zona pellucida and transduce pre-implantation embryos[37] (Fig. 4a). First, to establish the feasibility of using this approach for inducing gene knockouts in striped mice, we injected pregnant females carrying pre-implantation embryos with an rAAV packaged with Nme2Cas9 and single-guide RNA (sgRNA) expression cassettes directed to the coding sequence of *Tyrosinase* (*Tyr*), a gene essential for melanin production[38,39]. Visual inspection of pups coupled to genotyping revealed that this approach resulted in efficient gene editing, enabling us to generate complete knockout animals (Fig. 4b). To our knowledge, this is the first time that in vivo gene editing has been performed in a wild-derived mammalian species.

Encouraged by our proof-of-principle results, we next designed multiple sgRNAs against the 5′ coding region of *Sfrp2* (Extended Data Fig. 8a). We then tested each sgRNA in striped mouse immortalized dermal fibroblasts and chose the one that had the highest indel-inducing efficiency. Next, we injected an rAAV containing Nme2Cas9 and sg*Sfrp2* expression cassettes into the oviducts of plugged females. From a total of 21 females injected, we obtained 54 pups, 14 of which carried gene edits in *Sfrp2*. After mating F_0 founders and wild-type animals ($Sfrp2^{+/+}$) to ensure germline transmission, we crossed F_1 heterozygous animals ($Sfrp2^{+/-}$) to generate F_2 *Sfrp2* knockout ($Sfrp2^{-/-}$) mice. We used western blot to confirm the successful elimination of SFRP2 protein (Extended Data Fig. 8b). Next, to determine if *Sfrp2* knockout produces phenotypic changes in stripe width, as predicted by our mathematical model, we attempted to measure the distance between follicle regions in E16.5 embryos. However, because the stripe-like patterns by which hair follicles in striped mice develop do not provide clearly defined, consistent boundaries, measuring distances between the different dorsal regions in embryos is imprecise, obscuring potential differences in hair placode distribution (Extended Data Fig. 9a,b). Instead, we chose to quantify the resulting phenotypes in early postnatal stages, where pigmentation stripes can be used to reliably establish clear dorsal boundaries. Thus, as pigmentation stripes are already present at birth[11], we use their boundaries as a readout of a process occurring during development. Analysis of coat phenotypes from early postnatal (P3) stages revealed consistent differences in the coat patterns of F_2 $Sfrp2^{-/-}$ and $Sfrp2^{+/+}$ striped mice: we observed significant changes in the relative width of the stripes between $Sfrp2^{+/+}$ and $Sfrp2^{-/-}$ mice (Fig. 4c,d). Notably, the observed changes in stripe width are consistent with our model, which predicted subtle changes in this parameter in response to perturbations of the dorsoventral gradient (Fig. 3c,d). Hair length measurements indicated that $Sfrp2^{-/-}$ and $Sfrp2^{+/+}$ animals had similar differences between striped skin regions (Extended Data Fig. 9c). Thus, *Sfrp2* does not control the duration of the delay in follicle formation among

dorsal regions (that is, the amount of time when follicles are present in a region and absent in another) but rather regulates the spatial boundaries that define the positions of early and late forming follicles.

Altogether, the results from our in vivo genome editing experiment indicate that, by knocking out *Sfrp2*, the dorsoventral organizing gradient is perturbed, effectively altering the boundaries of the striped mouse's coat pattern.

Sfrp2 regulates pigmentation via activation of Wnt signalling

In addition to changes in stripe pattern, we noticed that mutant animals had obvious differences in coat coloration, with $Sfrp2^{-/-}$ mice showing overall lighter pigmentation than $Sfrp2^{+/+}$ mice (Fig. 4e, f). Previous studies have shown that pigment production/melanogenesis can be controlled by Wnt signals secreted from the dermal papilla[40,41], a specialized mesenchymal component of the hair follicle that signals to pigment-producing cells or melanocytes. Thus, to explore a potential link between *Sfrp2* and melanogenesis, we analysed the skin of striped mice at P4, a period in which pigment is being actively synthesized and deposited in the growing hair shaft. In situ hybridizations on skin sections revealed that *Sfrp2* was specifically and exclusively expressed in the dermal papilla, a pattern consistent with what is seen in laboratory mouse (Extended Data Fig. 10a)[23,24]. Next, to test the effect of *Sfrp2* expression on melanocytes, we stably transduced an immortalized mouse melanocyte cell line (Melan-A) with a lentiviral vector carrying the *Sfrp2* complementary DNA and used real-time quantitative PCR (RT–qPCR) to measure the expression of *Tyr* and *Mitf*, two genes that promote melanin synthesis[38,42]. Compared to melanocytes transduced with a control virus, cells overexpressing *Sfrp2* showed a significant increase in *Tyr* and *Mitf* (Extended Data Fig. 10b). Moreover, they also had marked increases in Wnt target genes, including *Axin2*, *C-myc* and *Ccnd1* (refs. 43–45). Notably, these results are consistent with previous findings, in which recombinant SFRP2 was found to induce melanin synthesis in human primary melanocytes, via Wnt signalling activation to promote darkening of skin explants[19].

Since *Sfrp2* promotes melanin synthesis in postnatal stages, we next asked whether expression levels of this gene differed between striped regions (that is, stripes of different colour). Using RT–qPCR measurements from dissected P4 stripe skin regions, we found that *Sfrp2* was significantly lower in the light stripes (R2) compared to the flanking dark stripes (R1 and R3) (Extended Data Fig. 10c), an expression pattern drastically different from the dorsoventral gradient during midembryogenesis. Indeed, a time-course analysis showed that *Sfrp2* expression in skin is temporally dynamic, shifting from a high–low dorsoventral gradient at E16.5 to the high–low–high pattern seen at P4 (Extended Data Fig. 10c). Taken together, our spatial expression data and in vitro functional experiments indicate that, during postnatal stages, *Sfrp2* undergoes a drastic shift in spatial expression and acts to promote melanogenesis via Wnt activation, thereby revealing an additional regulatory function during stripe pattern formation. Thus, *Sfpr2* regulates both the establishment of the prepattern and the implementation of the pigment pattern (Fig. 4g)

Evolutionary analysis of *Sfrp2*

Our experiments implicate *Sfrp2* as a crucial regulator of stripe patterns. Moreover, our comparative analyses between striped mouse and laboratory mouse revealed fundamental differences in the expression patterns of *Sfrp2*. We therefore carried out a series of experimental and computational analyses to gain insights into the processes shaping the evolution of *Sfrp2* in striped mice. First, we sought to establish whether the striped mouse *Sfrp2* coding sequence showed evidence of elevated substitution rates, as this could indicate changes in the function of the protein. Previously, we identified orthologous protein-coding transcripts across the genomes of the striped mouse and 23 other closely related murid species with publicly available assemblies (Fig. 5a) and performed analysis of relative evolutionary rates (RERs)[46], an approach that allows the identification of genes showing accelerated evolution relative to the per species background rate. Re-examination of our RER dataset revealed that *Sfrp2* did not show evidence of strong evolutionary acceleration compared to background rates of coding gene evolution (Fig. 5b). In agreement with this, we did not detect evidence that the striped mouse *Sfrp2* coding sequence has evolved under positive selection, as determined by the K_a/K_s-based, branch-site model ($P > 0.05$; Supplementary Table 2)[47]. Thus, these analyses indicate that the striped mouse *Sfrp2* coding sequence has not experienced lineage-specific changes that may account for the evolution of stripe patterns.

Given our model that it is temporal and spatial differences in *Sfrp2* expression levels that contribute to the evolution of stripe patterns, it is not surprising that changes in the *Sfrp2* coding sequence were not identified. Rather, it is more likely that the differences in *Sfrp2* between striped mouse and laboratory mouse have originated via changes in *cis*-regulatory elements (CREs), as these sequences play key roles controlling the spatiotemporal expression of genes. To probe into this, we performed a multispecies comparative analysis of the *Sfrp2* regulatory region. We first generated transposase-accessible chromatin sequencing (ATAC-seq) data from embryonic (E15.5) dorsal laboratory mouse skin with the goal of identifying candidate CREs that we could then compare across species. Using an orthologue identification and processing pipeline derived from the one used in our coding gene analyses, we lifted the sequences under these peaks over to the genomes of the striped mouse and of the grass rat (*Arvicanthis niloticus*), which is the striped mouse's sister species (Fig. 5a). Since the grass rat does not have stripes, including this species in our comparative analysis allows us to distinguish CREs that are present in the most recent common ancestor of striped mouse and grass rat from those that evolved uniquely in striped mouse and are therefore correlated with the presence of stripes (Fig. 5a). Using computational analyses, we independently searched for the candidate CREs that were closest to *Sfrp2* in each of the three species (laboratory mouse, striped mouse and grass rat). Our analysis identified a total of five distinct candidate CREs located upstream and downstream of the *Sfrp2* coding sequence. Interestingly, these regions showed a high degree of synteny across the three species (Fig. 5c). After aligning the orthologous sequences, we performed computational scans of transcription factor (TF) binding sites and found that the five different candidate regulatory regions were enriched for the same set of TF-binding motifs across the three species (Supplementary Table 3). Despite this overall conservation in

enriched binding motifs, however, close inspection of the different candidate CREs revealed marked differences between the striped mouse and the other two species. Specifically, three of the five CREs had insertions or deletions (indels) that were uniquely present in the striped mouse (Fig. 5c and Supplementary Table 4). Notably, these indels contained several predicted TF-binding motifs (Fig. 5c). For example, CRE_2 and CRE_5 showed different striped mouse-specific insertions containing consensus motif sequences for several TFs (for example, *Sox5*, *Hoxd10*, *Lhx3*, *Sox13* and *Prdm1*), all of which are expressed in our striped mouse RNA-seq dataset (Supplementary Data 1 and Supplementary Table 4). Similarly, CRE_2 and CRE_4 had striped mouse-specific deletions predicted to remove binding motifs for TFs such as *Pax1*, *Pax6* or *Ets1*, among others (Supplementary Table 4). As genomic changes in TF-binding motifs can alter gene expression domains, the indel patterns observed here may explain the unique *Sfrp2* expression patterns seen in striped mice. Our future efforts will be directed towards validating whether the regulatory differences observed here lead to functional differences in *Sfrp2* expression.

Taken together, the results from our evolutionary analysis of closely related rodents suggest that, while the striped mouse has not experienced significant changes in the *Sfrp2* coding sequence, this species has evolved lineage-specific changes in CREs surrounding *Sfrp2*, many of which may be implicated in modulating the expression patterns of this gene.

Discussion

In birds and mammals, periodic pigment patterns arise from two sequential processes: the first occurs early in embryogenesis and specifies the positional boundaries of the future pattern (pattern establishment or prepattern); the second implements this prepattern through genes mediating pigment production during hair growth and cycling, giving rise to the observed colour differences (pattern implementation)[4,12,48]. Here, we identify *Sfrp2* as a regulator of both the establishment of the prepattern and its implementation, a dual role that is made possible by its dynamic expression pattern throughout embryogenesis and early postnatal stages, as well as its opposing effects on Wnt signalling (Fig. 4g). The involvement of *Sfrp2* at multiple stages of pattern formation implies a fine-tuned spatiotemporal regulatory control, probably achieved through a complex *cis*-regulatory architecture and the action of multiple binding factors[49].

Our results contrast with what is seen in felids, where the molecular factors regulating pattern establishment are different from the ones controlling the implementation events that follow[10]. Moreover, while *Dkk4* prefigures the coat patterns of domestic cats and is expressed periodically in embryonic cat skin[18], we don't find evidence that *Dkk4* or any other gene is expressed in a periodic, stripe-specific pattern during striped mouse embryogenesis (Extended Data Fig. 1). Thus, coat patterning mechanisms among rodents and felids are fundamentally different. Despite these marked differences, however, it is interesting that different components of the Wnt signalling pathway (*Sfrp2* and *Dkk4*) have independently converged to regulate the coat patterns of striped mice and cats.

Secreted frizzled-related proteins (SFRPs) are known regulators of Wnt signalling that can exert their effects through a wide variety of mechanisms, including Wnt ligand sequestering,

binding to Frizzled receptors, stabilization of Wnt–Frizzled complexes and direct activation of Frizzled[18]. As such, SFRPs can either inhibit or activate Wnt signalling and their effect is dependent on cell type, developmental stage and cellular microenvironment[11]. In striped mice, embryonic expression of *Sfrp2* in a subset of dermal fibroblasts causes a decrease of epidermal CTNNB1 and LEF1, leading to alterations in placode number (Fig. 4g). Later in development, dermal papilla-specific expression of *Sfrp2* alters melanocyte behaviour, causing an increase in the expression of Wnt targets and genes involved in melanogenesis (Fig. 4g). Thus, our results show that *Sfrp2* can lead to opposing regulation (activation and inhibition) of Wnt signalling within the same tissue.

It is noteworthy that elimination of *Sfrp2* led to subtle, albeit consistent differences in the coat pattern of striped mice. This result is not surprising, as subtle changes in stripe width are consistent with predictions from our simulations. Moreover, it is likely that there are additional reinforcing/redundant mechanisms at play that act in concert to establish the dorsoventral orienting gradient and assure phenotypic robustness. For example, our bulk-level RNA-seq data from E16.5 embryos show that there are additional Wnt modulators which are also expressed in a dorsoventral gradient, such as *Dkk2*, *Igfb4*, *Rspo2* and *Rspo4* (Extended Data Fig. 2 and Supplementary Data 1). Such molecules may act in coordination with *Sfrp2* to specify patterns of placode morphogenesis and are therefore still playing a substantial role in regulating this trait in $Sfrp2^{-/-}$ striped mice. We note, however, that while our analyses suggests that *Sfrp2* acts to regulate patterns of hair placode formation, our experimental measurements from *Sfrp2* knockout animals are taken from individuals at early postnatal stages (P3), rather than from embryonic time points. In this regard, as stripes are already present at birth[11,41], we use pigmentation stripes as a readout of a developmental process. Thus, an assumption of our work is that the changes observed in early postnatal stages are representative of changes occurring in placode patterning.

With respect to pigmentation, our previous work showed that hair colour differences in striped mice are controlled by the interplay of melanocyte-autonomous (for example, *Alx3*-mediated suppression of melanocyte differentiation) and non-autonomous processes (for example, regulation of pigment-type switching by paracrine factors secreted from the dermal papilla, including *Asip* and *Edn3*)[11]. Thus, although *Sfrp2* influences pigmentation, as our experiments show, it is clear that modulation of hair colour in striped mice is achieved through the combinatorial effect of multiple genes[49].

In conclusion, by integrating multidisciplinary approaches, our work reveals insights into the mechanisms by which spatial patterns are established in developing embryos and exemplifies how the molecular basis of a naturally evolved phenotypic trait can be dissected in an emerging model species.

Methods

Striped mouse husbandry

The F_{10} descendants of wild-derived striped mice (*R. pumilio)*, originating from Goegap Nature Reserve, South Africa, 29° 41.56′ S, 18° 1.60′ E, were originally obtained from a captive colony at the University of Zurich (Switzerland) and are maintained at Princeton

University. *R. pumilio* are kept at a 16:8 light:dark cycle and given 4 g of food per animal daily. All experiments performed were approved by Princeton University's Institutional Animal Care and Use Committee.

Laboratory mouse husbandry

All laboratory mouse (*M. musculus*) experiments were carried out using the 129S2/SvPasCrl strain, obtained from Charles River Laboratories. All experiments were approved by Princeton University's Institutional Animal Care and Use Committee.

Embryo staging

To create a developmental time series of striped mouse embryonic development, embryos spanning midgestation were collected and ordered chronologically, on the basis of embryo size and various morphological features including eye pigmentation, webbing of the forelimb and hindlimb skull morphology[50]. The stage at which epidermal hair placodes first become visible in striped mice was considered 'stage matched' to *Mus* E15.5, the stage at which hair placodes first become visible by eye in *Mus*. Indeed, other morphological features in striped mice at this stage agreed remarkably well with that of E15.5 laboratory mouse embryos. This stage in striped mice was later confirmed to be E16.5 via a combination of vaginal cytology and ultrasound imaging. Staging of all striped mouse embryos was confirmed using vaginal cytology and ultrasound imaging.

Sample preparation for in situ hybridization and immunofluorescence

Pregnant females of the appropriate stage were killed following approved protocols. Embryos were harvested, fixed in 4% paraformaldehyde (PFA), dehydrated in increasing concentrations of methanol/ PBS (25%, 50%, 75% and 100%) and stored at −20 °C.

For whole-mount in situ hybridizations, embryos were rehydrated in decreasing concentrations of methanol/PBT (75%, 50% and 25%) and washed with PBS. For section in situ hybridizations and immunofluorescence, embryos were rehydrated as described above and then incubated in 10% sucrose overnight at 4 °C, followed by a 30% sucrose overnight incubation at 4 °C. Embryos were then incubated in 50% sucrose, 50% optimal cutting temperature (OCT) compound for 3 h at room temperature, embedded in OCT, flash frozen and cryosectioned (16 μm thickness) using a Leica CM3050S Cryostat. Slides were frozen at −80 °C until use.

Whole-mount in situ hybridizations

Messenger RNA sequences for target genes were obtained either from the National Center for Biotechnology Information (NCBI) (*M. musculus*) or a de novo transcriptome (*R. pumilio*). For *R. pumilio*, we generated the following antisense riboprobes: *Dkk4* (543 base pairs (bp)), *Wif1* (563 bp), *Bmp4* (619 bp), *Wnt10b* (360 bp), *Dkk1* (546 bp) and *Ctnnb1* (400 bp). For *M. musculus*, we generated a *Dkk4* probe (550 bp). All primer sequences are reported in Supplementary Table 5. All probes were sequence-confirmed using Sanger sequencing. Whole-mount in situ hybridizations were then performed using previously described protocols[51]. Briefly, embryos were post-fixed with 4% PFA in PBS, washed with PBS, treated with 20 μg ml^{-1} of proteinase (MilliporeSigma, P2308) in PBT

for 45 min and incubated overnight with riboprobes at 65 °C. The following morning, probes were washed with MABT (maleic acid, NaCl, Tween-20) and incubated overnight with secondary anti-DIG (MilliporeSigma, 11333089001; 1:2,000) diluted in MABT, 2% Boehringer Blocking Reagent (MilliporeSigma, 11096176001) and 20% heat-treated sheep serum. After washing several times with MABT, the signal was developed by incubating with NBT/BCIP (MilliporeSigma, 11697471001). Once signal had developed sufficiently, the reaction was stopped by washing several times with PBT and fixing in 4% PFA overnight. Embryos were visualized using a SMZ18 stereo microscope (Nikon). At least three embryos per probe per species were analysed.

Bulk-level RNA-seq

E16.5 striped mouse embryos ($n = 3$) were harvested from pregnant females and placed in 1× PBS on ice. Regions R1 (dorsal-most, placode-barren), R2 (dorsal-most, placode-rich), R3 (ventral-most, placode-barren) and R4 (ventral-most, placode-rich) were microdissected using morphological placodes as reference points. Regions from both sides of the midline were combined into a single tube containing 500 µl of RNALater (Thermo Fisher Scientific AM7020) and stored at −20 °C until RNA extraction. RNA was extracted using the RNeasy fibrous tissue mini kit (QIAGEN) per the manufacturer's protocol. RNA-seq libraries were prepped using the TruSeq RNA Library Prep kit v.2 (Illumina, RS-122–2001) and sequenced on a NovaSeq 6000 (2× 65 bp, paired-end). Pairwise differential expression analyses between the transcriptomes of dorsal skin regions R1–R4 were performed using DeSeq2 v.1.30.1 from BioConductor (https://bioconductor.org/)[52]. Only genes differentially expressed with $P_{adj} < 0.05$ were considered. For visualization of all comparisons simultaneously, UpSet plots were generated using UpSetR[53].

Modelling stripe patterns of placode formation

All simulations in our numerical study were carried out on a domain of [−1,1]. Throughout, we used values of $D_M = 1$, $k_M = 1$, $l = 0.5$, $M_0 = 1$ and $\epsilon = 10^{-2}$. Simulations were performed using the Dedalus package for spectral pde solution with a discretization of 512 modes[54]. Steady-state solutions in each case were calculated via a variant of Newton's method stability of stripes and uniform states were determined by calculation of the largest eigenvalues[55] and a timestep of $dt = 0.01$.

The plots of concentration profiles in Fig. 3c and in Extended Data Fig. 7 are some of the stable steady states calculated by this method, based on starting guesses with either uniform concentrations or four stripes. As noted in the main text, the (nearly) uniform steady states identified by this method were only stable at small values of a regardless of our model choice. The rightmost panel of Fig. 3c was generated through a continuation of a four-stripe steady state as the parameter a was varied from zero to one under model variant 1 (refs. 55). For all cases, these steady states were stable. Other steady stable steady states involving alternate numbers of stripes likewise exist but a full bifurcation analysis of this problem is beyond the scope of the current paper.

scRNA-seq

Sample preparation and library generation.—Embryos from *R. pumilio and M. musculus* females were harvested at the relevant stages of pregnancy (E12.5–E15.5 for *M. musculus*; E13.5–E16.5 for *R. pumilio*). For all stages (except *R. pumilio* E16.5, see below), a single, rectangular piece of dorsal skin, symmetrical across the midline, was microdissected, using the forelimbs and hindlimbs as reference points to maintain consistency across stages and species. For *R. pumilio* E16.5 embryos, regions R1 (dorsal-most, placode-barren), R2 (dorsal-most, placode-rich) and R3 (ventral-most, placode-barren) were microdissected using morphological placodes as markers and regions from both sides of the midline were combined. Dorsal skins from three embryos were pooled (with the exception of *M. musculus* E13, $n = 2$) into a single tube containing 1 ml of 0.25% trypsin/PBS. Skins were minced with fine scissors and transferred to an Eppendorf tube containing 10 ml of 0.25% trypsin (Thermo Fisher Scientific, 25200072)/PBS. Tubes were incubated at 37 °C in a hybridization oven with gentle rotation for 15–30 min (timing was dependent on embryonic stage) until the tissue was well dissociated. Primary cell suspensions were passed through a 70 μm filter and diluted 1:5 with 4% bovine calf serum (BCS, Thermo Fisher Scientific, SH3007203)/PBS. Cells were centrifuged at 300*g* in a refrigerated centrifuge set at 4 °C for 10 min. Supernatant was discarded, the cell pellet was gently washed with 4% BCS/PBS and resuspended in 100 μl of 0.1% ultrapure bovine serum albumin (BSA; Thermo Fisher Scientific, B14)/PBS. Cell number and viability were assessed using trypan exclusion and a TC20 automated cell counter (BioRad). The scRNA-seq libraries were generated using the Chromium Single Cell 3′ Reagent Kits (v.2) (10x Genomics) following the manufacturer's instructions. Libraries were sequenced on an Illumina NovaSeq 6000 (25× 125 bp, paired-end)

***R. pumilio* annotation.—**To generate gene annotations for the striped mouse genome suitable for analysis of bulk RNA-seq data, we transferred high-quality NCBI gene annotations from the laboratory mouse (Mus_musculus.GRCm38.100.chr.gff3) to the de novo *R. pumilio* assembly[46]. To accomplish this, we used a homology-based lift-over procedure, implemented by the program Liftoff v.1.4.1 using default parameters. Raw reads, genomes annotations have all been deposited under BioProject: PRJNA858857 and BioSample: SAMN29758252.

Generation of a 'rhabdomyzed' genome.—To both facilitate comparisons of transcriptomic data between *R. pumilio* and *M. musculus* to leverage the high-quality gene annotations available for the latter, we generated an alternative, reference-guided assembly for the *R. pumilio* genome against which sequencing data were analysed using previously described methods[56]. Briefly, genome reads for *R. pumilio* were aligned against the GRCm38 *M. musculus* genome using bwa-mem2 v.2.1. Alignments were sorted and duplicates were removed with SortSam and MarkDuplicates from Picard tools (http://broadinstitute.github.io/picard/). Next, read pileups were generated using bcftools v.1.11 programs mpileup, ignoring indels to preserve the reference GRCm38 coordinate system. Base calls were then generated using the bcftools call multi-allelic caller. Finally, an initial reference-guided assembly was generated by projecting striped mouse base calls onto the reference mouse genome with bcftools consensus. This procedure was then repeated once

more using the resulting consensus sequence from the first round as the new starting reference genome. Metrics using the 'rhabdomyzed' genome compared favourably (for example, number of cells identified, median genes identified per cell percentage of genes confidently mapped to transcriptome) to a *R. pumilio* assembly/lift-over annotation and was thus chosen for downstream analyses.

Processing of raw scRNA-seq data.—Raw FASTQ reads from *R. pumilio* samples were mapped with Cell Ranger (v.3.1.0) to the rhabdomyzed *Mus genome* (see above): (Rhabdomys_to_Mus_bcftools_consensus3. fa/Mus_Musculus.GRCm38.101.gtf)

Raw FASTQ reads from *M. musculus* samples were mapped with Cell Ranger (v.3.1.0) to the *M. musculus* mm10 reference genome (GRCm38.94.dna/GRCm38.84.gtf). Raw FASTQ reads will be deposited in BioProject.

Doublet/multiplet simulation and low-quality cell filtering.—Raw count matrices from *R. pumilio* and *M. musculus* obtained from alignment with the rhabdomyzed *Mus* genome or mm10 reference genome, respectively, were preprocessed and doublet/multiplets were simulated using single-cell remover of doublets (Scrublet)[57] (v.0.2.1) with default parameters enabled. The doublet/multiplet score threshold was adjusted manually to intersect the bimodal distribution of the observed transcriptomes on the probability density histogram as suggested. Putative singlets were kept and used for downstream query and comparative analyses if and only if they met the following user-defined collective quality control metrics filtering criteria: (1) cells with >350 but <5,000 genes were kept; (2) cells containing <10% total mitochondrial gene content were kept; (3) cells not identified as outliers falling outside a prediction confidence interval defined by a quadratic in a model of a gene versus counts plot ($P = 1 \times 10^{-3}$) were kept[58].

Anchoring, integration downstream analysis of scRNA-seq data.—We performed anchoring and integration of *R. pumilio* or *M. musculus* datasets using the Seurat package (v.3.2.2, R Studio v.3.6.1)[59]. In brief, species-specific Seurat objects were created using individual, raw digitized count matrices as suggested by developer. Objects were merged and individual gene expression matrices were normalized variable genes/features identified. Datasets were anchored ($n = 30$ dimensions) and integrated ($n = 30$ dimensions). The integrated object was then scaled. Significant principal components (PCs) used for clustering and neighbour-finding were identified using a combination of statistical and heuristic methods. Neighbours and clusters were identified with dimensions specified by user and visualized using two-dimensional *t*-distributed stochastic neighbour embedding (*t*-SNE). For all analysis, R1, R2 R3 from *R. pumilio* E16.5 embryos were randomly down-sampled to equal cell numbers before integration into a single object that was representative of E16.5 *R. pumilio* dorsal skin.

Cell-type annotation.—Cell types in *R. pumilio* and *M. musculus* were defined and annotated using a core set of bona fide E14.5 *M. musculus* gene biomarkers[23,25,26,60] and are reported in Supplementary Table 1 and in Extended Data Fig. 3. Aggregate biomarker gene module scores were computed in Seurat. Aggregate biomarker gene module scores and

individual gene expression profiles were log-normalized and visualized as feature plots in two-dimensional *t*-SNE embedding.

Quantification of *Sfrp2*$^+$ fibroblasts.—To quantify the number of *Sfrp2*$^+$ fibroblasts in *R. pumilio* and *M. musculus*, we randomly subsampled *Sfrp2*$^+$ fibroblasts ($Sfrp2_{\text{normalized counts}} > 0$) in *R. pumilio* or *M. musculus* ($n = 25$ iterations). To mitigate potential differences owed to sample size, we subsampled fibroblasts to the lowest number of total fibroblasts in any one comparison. *Sfrp2*$^+$ fibroblasts in *R. pumilio* or *M. musculus* were then normalized to total fibroblasts. Results from each iteration are plotted with confidence intervals and their correlation was determined with Spearman's correlation. Results are represented as the average ratio of *Sfrp2*$^+$ fibroblasts to total fibroblasts from 25 different iterations ± s.d.

Gene expression analysis.—To quantify gene expression changes in *R. pumilio* fibroblasts that correlate with *Sfrp2* expression levels, we performed three subsamplings of fibroblasts based on *Sfrp2* UMI counts: (1) *Sfrp2*-high >1.0 and *Sfrp2*-low <1, (2) *Sfrp2*-high >2 and *Sfrp2*-low <2 and (3) *Sfrp2*-high >3 and *Sfrp2*-low <3. Gene expression analysis was performed in Seurat (two-sided Wilcoxon rank sum test) to identify differentially expressed genes (DEGs, $P_{\text{adj}} < 0.05$). Although good agreement was observed in all subsamplings used, only genes identified as differential in all three subsamplings were subjected to gene ontology analysis using Enrichr and significant GOs ($P_{\text{adj}} < 0.05$) were considered.

In situ hybridization chain reaction

A conserved region in the *Sfrp2* mRNA between *R. pumilio* and *M. musculus* was used to generate 16 probe binding sequences for in situ hybridization chain reaction (HCR). HCR was performed using the standard protocol for fixed frozen tissue sections available from Molecular Instruments. High signal within limb sections of both species was used as a positive control. At least three embryos per species were analysed.

Immunofluorescence

Immunofluorescence was performed on tissue sections using standard procedures. Briefly, slides were washed with 1× PBS with 0.1% Tween (PBT) and blocked with 1× PBT/3% BSA for 1 h. Primary rabbit anti-LEF1 (Cell Signalling no. 2230 S, 1:100), rabbit anti-β-catenin (MilliporeSigma, C2206, 1:500), chicken anti-GFP (Novus Biologicals no. NB100–1614, 1:200) or rabbit anti-Krt14 (BioLegend, 905301, 1:1,000) were diluted in 1× PBT/3% BSA and slides were incubated at 4 °C overnight. The next morning, slides were washed several times with 1× PBT and secondary antibodies (goat anti-mouse Alexa Fluor 488, Thermo Fisher, A-21133 or goat anti-mouse Alexa Fluor 546, Thermo Fisher, A-11001) were diluted 1:500 in 1× PBT/3% BSA and slides were incubated for 1 h at room temperature. Slides were washed several times with 1× PBT, stained with DAPI to visualize nuclei mounted for imaging. Images were taken on a Nikon A1R confocal microscope. At least three embryos per condition were analysed.

Generation of *Rosa*$^{Sfrp2\text{-}GFP}$ laboratory mice

Srfp2 cDNA was synthesized (Azenta) and cloned into pR26 CAG/T2AGFP Asc (pR26 CAG/GFP Asc was a gift from R. Kuehn, Addgene plasmid no. 74285 and modified to contain a T2A instead of IRES). Thus, the resulting plasmid contains the CAG promoter, a loxP flanked stop cassette, the *Sfrp2* cDNA, a T2A site and GFP. The plasmid was inserted into the *Rosa26* locus by CRISPR–Cas9-mediated gene targeting. Cas9 (IDT) was complexed with an sgRNA (MilliporeSigma) having the spacer sequence 5′-ACTCCAGTCTTTCTAGAAGA-3′. C57BL/6J zygotes were microinjected and transferred into pseudopregnant recipients. Founders were screened for the presence of GFP by PCR using primers GFP(F) and GFP(R). Twelve founders were further screened for 5′ end targeting using primers ROSA26J and SAR and for 3′ end targeting using GFP(F) and ROSA26L. All 12 were correctly targeted, 10 were chosen to confirm the presence of the cDNA by Sanger sequencing. Through subsequent breeding, the transgene was introduced into the 129S2/SvPasCrl background, where all experiments were carried. Primer sequences are available in Supplementary Table 5.

Quantification of hair follicle number

To examine the effect of dermal *Sfrp2* overexpression on hair follicle number, *Rosa*$^{Sfrp2\text{-}GFP}$ females were crossed to *Dermo1-Cre* (JAX stock no. 008712) males and embryos were collected at E17.5. Embryos were fixed, embedded and immunostained for GFP, as described above. GFP expression was mosaic but a posterior dorsal region consistently showed high levels of GFP signal across all GFP (+) embryos. Within this region, follicle quantification was performed on equally sized areas of the skin after performing haematoxylin–eosin stains to reliably identify hair follicles. In total, four double-transgenic and four control embryos were quantified. For each embryo, hair follicle numbers from four skin sections were counted and averaged with an equal sized region of the embryo. Statistical significance was assessed using an unpaired *t*-test, two-sided. Statistical significance was assigned *$P < 0.05$; **$P < 0.01$, ***$P < 0.001$ and ****$P < 0.0001$.

Real-time quantitative PCR

Individual dorsal skin regions R1–R3 were dissected using either hair placodes (E16.5), hair length (E19.5) or pigmentation (P0, P4) as markers. Skin sections were stored in 500 μl of RNALater (Thermo Fisher Scientific, AM7020) and kept at −20 °C until RNA extraction.

RNA was extracted using the RNeasy fibrous tissue mini kit (QIAGEN) per the manufacturer's protocol. The cDNA synthesis was carried out using qScript cDNA SuperMix (Quantabio) and RT–qPCR for *Sfrp2* was performed using SYBR Green RT–qPCR Reagent (Quantabio, 95054–500) on a ViiA 7 Real-Time PCR machine (Applied Biosystems). Primers used for RT–qPCR are listed in Supplementary Table 5.

Overexpression of *Sfrp2* in melanocytes

The lentivirus construct used in this study is derived from the LV-*GFP*[61]. To generate LV-*SFRP2-GFP*, we amplified the *Sfrp2* coding sequence from an *Sfrp2* (NM_009144) Mouse Tagged ORF Clone (Origene catalogue no. MR204070) using CloneAmp HiFi PCR Premix (Takara 639298) and cloned it (in frame) into the linearized LV-*GFP* plasmid using

In-Fusion Snap Assembly Master Mix (Takara no. 638947). Large-scale production of VSV-G pseudotyped lentivirus was carried out using calcium phosphate transfections of 293FT cells and the helper plasmids pMD2.G and psPAX2 (Addgene plasmids 12259 and 12260). Before transfection, Melan-A cells (purchased from the Wellcome Trust Functional Genomics Cell Bank at St. George's, University of London) were seeded in RPMI 1640 media supplemented with penicillin (100,000 U l^{-1}), streptomycin (100 mg l^{-1}), fetal bovine serum (10%) and tetradecanoyl phorbol acetate (MilliporeSigma, P3766) (200 nM). At ~80% confluency, cells were centrifuged for 30 min at 37 °C and media were aspirated away and replenished with fresh media lacking antibiotics. LV-*GFP* or LV-*SFRP2-GFP* viral supernatant was added to each well along with a 1 mg ml^{-1} polybrene diluted in bovine calf serum. Plates were gently swirled and incubated at 37 °C/5% CO_2 for 30 min. Plates were then centrifuged at 1,100*g* for 30 min at 37 °C. Media were removed, cells were rinsed twice with PBS and fresh media added. To enrich for cells with high transfection efficiency, cells with high GFP expression were sorted by fluorescence-activated cell sorting on a BD FACSAria II (BD Biosciences), grown to confluency, sorted one additional time and grown to ~80% confluency. Media were removed, cells were incubated in 500 µl of TriReagent (Zymo, R2050–1-200) for 5 min, flash frozen in liquid nitrogen and stored at −80 °C. RNA was isolated using a direct-zol RNA microprep kit (Zymo R2062). The cDNA synthesis was carried out using qScript cDNA SuperMix (Quantabio, 95048–100) and RT–qPCR for *Mitf*, *Tyr*, *Axin2*, *C-myc* and *Ccnd1* and was performed using SYBR Green RT–qPCR Reagent (Quantabio, 95054–500) on a ViiA 7 Real-Time PCR machine (Applied Biosystems), as described above.

In vivo genome editing in *R. pumilio*

Generation of immortalized *R. pumilio* fibroblasts.—A skin biopsy was obtained from the flank of an adult male *R. pumilio* and dermal fibroblasts were subsequently isolated following a previously published protocol[62,63]. In brief, hair, fat and connective tissue were scraped away from the biopsy before digesting overnight at 4 °C in HBSS without Ca^{2+} and Mg^{2+} (Thermo Fisher, 88284) containing dispase at a final concentration of 500 caseinolytic units ml^{-1} (Corning, CLS354235) and an antibiotic/antimycotic solution final concentrations of 100 µg ml^{-1} of streptomycin, 100 IU ml^{-1} penicillin and 250 ng ml^{-1} amphotericin B (HyClone, SV30079.01). Following digestions, the epidermis was removed and discarded. The dermis was cut into small pieces, moistened with Dulbecco's modified Eagle medium (Thermo Fisher; DMEM, 119965092) and pressed into grooves scored into the wells of a six-well tissue culture dish. The dermis was maintained in DMEM containing 10% (vol/vol) fetal bovine serum (Omega Scientific, FB-01) and 1% (vol/ vol) penicillin/streptomycin (Corning, 30–002-Cl) at 37 °C, 5% (vol/vol) CO_2. Media were changed every 4–5 days and cultures monitored for fibroblast growth. Once sufficient outgrowth had occurred, the dermis was removed from the plate and the fibroblasts removed by trypsinization (0.05% trypsin-EDTA; Thermo Fisher Scientific, 25300054) for expansion into larger culture dishes.

To generate the immortalized dermal fibroblast cell line, γ-retroviral pseudoparticles containing a transfer plasmid encoding Simian virus 40 (SV40) large T antigen were produced in HEK293T cells. Cells were cultured on poly-L-lysine−coated 10 cm plates at 37 °C, 5% (vol/vol) CO_2 in 10% FBS DMEM. At ~80% confluency, Xtremegene HP DNA

transfection reagent (MilliporeSigma, 6366244001) was used per manufacturer's directions to cotransfect the cells with 4 μg of pBABE-neo-SV40 large T, a generous gift from B. Weinberg (Addgene plasmid no. 1780); 4 μg of a plasmid containing the genes for Moloney murine leukaemia virus gag-pol; and 0.57 μg of a plasmid containing the gene for the G envelope protein of vesicular stomatitis virus. Supernatants were harvested 24, 48 and 72 h post-transfection, stored at 4 °C then pooled before passing through a 0.45 μm membrane filter (MilliporeSigma, HAWP02500). Polybrene (Sigma-Aldrich, TR-1003; final concentration, 4 μg ml^{-1}) and HEPES (Gibco, 15630080; final concentration, 2 mM) were added to the filtered supernatants; aliquots were prepared and at −80 °C until needed. Primary dermal fibroblasts were seeded in six-well plates for transduction so that cell confluency was 30–40% at the time of transduction. The cells were 'spinoculated' in a centrifuge at 37 °C, 931 relative centrifugal force (r.c.f.) for 2 h with 2 ml of thawed, undiluted γ-retroviral pseudoparticles per well. The cells were subsequently kept at 37 °C, 5% (vol/vol) CO_2 and the media replaced with 10% FBS DMEM 6 h post-spinoculation. The transduced cells were pooled once they achieved ~80% confluency in the six-well plate and subsequently expanded to prepare immortalized cell stocks. Cells were verified as negative for mycoplasma by testing with the MycoAlert Mycoplasma Detection Assay kit (Lonza, LT07–318) per the manufacturer's instructions.

Guide-RNA design and testing.—We designed nine CRISPR sgRNAs targeting the *R. pumilio Sfrp2* exon1 using CRISPOR[64]. We then cloned each guide into the rAAV Nme2*Cas9* plasmid by replacing sg*Tyr* with sg*Sfrp2* (refs. 37). Next, we transfected each rAAV into immortalized striped mouse immortalized fibroblasts using lipofectamine3000 (L300008, Thermo Fisher). At ~3–4 days post-transfection, we extracted genomic DNA using the Zymo Quick DNA Miniprep Plus Kit (Zymo) and performed targeted PCR on *Sfrp2* (primers are listed in Supplementary Table 4). We then performed a T7E1 nuclease assay (M0302, New England Biolabs) according to the manufacturer's protocol and resolved digested products on a 1.2% agarose gel containing STBY safe DNA gel stain (Invitrogen) to assess excision efficiency of each designed sgRNA.

rAAV production, in vivo transduction genotyping.—The rAAV6. Nme2*Cas9*.sg*Sfrp2* was produced, concentrated and purified by the PNI viral core facility at Princeton University. Female *R. pumilio* between 4 and 6 months of age were chosen to breed with age-matched males. The presence of vaginal mating plugs or sperm was designated as days post coitum (d.p.c) 0.5. Pregnant females at d.p.c. 0.75 ($n = 21$) were anaesthetized, administered with analgesics and aseptically prepared for survival surgery. To deliver rAAV, we slowly injected 0.5–1 μl of rAAV (1–3 × 10^9 genome copy) mixed with Chicago Sky Blue dye (0.1%, Fisher Scientific, catalogue no. AAA1424214) into the oviduct ampulla using a glass micropipette with tip diameter of ~10–30 μm. The injection technique in *R. pumilio* was optimized on the basis of a technique reported in *M. musculus*[37]. Operated animals were allowed to carry to term and pups were genotyped as follows. We collected ear punch tissue from individual animals and extracted genomic DNA using a Zymo Quick DNA Miniprep Plus Kit (Zymo). Next, we PCR-amplified the genomic region containing the guide targeting site (primers are listed in Supplementary Table 4) and resolved PCR amplicons using agarose gel electrophoresis. For F_0 striped mice,

PCR amplicons were further cloned into a pSC-amp/kan vector using StrataClone PCR cloning kit (240205, Agilent Technologies). We picked ~20–50 single colonies per sample to determine the presence, composition and frequency of targeted mutations via Sanger sequencing.

For knocking out *Tyr* in *R. pumilio*, six F_0 founders were mated to wild-type animals to obtain germline transmission. Of these six founders, all of them successfully produced heterozygous animals.

For knocking out *Sfrp2* in *R. pumilio*, 11 F_0founders were mated to wild-type animals to obtain germline transmission. Specifically, we selectively isolated four mutated alleles (2, 13, 466 and 527 bp deletions) for subsequent experiments. Ten out of 11 founders tested successfully produced heterozygous F_1 animals. F_1 heterozygous striped mice containing the same mutated alleles were crossed to produce F_2 animals. Genotypes of all F_2 animals were determined by a combination of PCR, TOPO cloning and Sanger sequencing. At least two independently generated null alleles were tested in phenotypic analyses. Our designation of $Sfrp2^{-/-}$ mice encompasses animals that either share the same mutated allele or have a combination of two different mutated alleles.

Western blots.—We collected fresh liver tissues of killed animals and prepared protein lysates in RIPA (50 mM Tris-HCl pH 8.0, 150 mM NaCl, 0.1% SDS, 0.5% sodium deoxycholate, 0.1% Triton-X, 1 mM EDTA) supplemented with protease inhibitor cocktail (ab271306, Abcam). Protein concentration was quantified by Pierce Detergent Compatible Bradford Assay (Thermo Fisher Scientific, 23246). For SDS–polyacrylamide gel electrophoresis, we loaded 20 μg of total protein per sample. Membranes were probed with primary antibodies at 4 °C overnight, washed with TBST 4× and incubated in secondary antibody for 1 h at room temperature. Primary antibodies: 1:100 *Sfrp2* (ab137560, Abcam) and 1:1,000 β-tubulin (mAb 86298, Cell Signalling). Secondary antibodies: 1:20,000 IRDye 800CW Goat anti-Rabbit IgG (926–32211, LI-COR Biosciences) and 1:20,000 IRDye 680RD Goat anti-Mouse IgG system (926–68070, LI-COR Biosciences). Membranes were developed using an Odyssey CLx imaging system (LI-COR Biosciences).

Quantification of $Sfrp2^{-/-}$ phenotypes

Stripe width in embryos.—Equally staged E16.5 striped mouse $Sfrp2^{-/-}$ ($n = 3$) or $Sfrp2^{+/+}$ ($n = 3$) embryos were stained for *Dkk4* and photographed using a Nikon SMZ18 dissecting microscope. To quantify stripe width, FIJI (ImageJ) was used to draw line segments spanning each region of interest (ROI; R1 and R3). For each image, five horizontal lines connecting hair placodes were traced and the length of the lines was recorded. For each region, an average width was calculated. Since hair follicles do not form in a regular pattern that follows a clearly delineated and continuous line along the anteroposterior axis, the boundaries between dorsal regions are extremely irregular, making it difficult to establish where the measurements should start and end. As this is especially evident in R2, we restricted our analysis to R1 and R3.

Stripe width in pups.—Dorsal skin from equally staged P3 striped mouse *Sfrp2*$^{-/-}$ ($n = 7$) or *Sfrp2*$^{+/+}$ ($n = 10$) pups was dissected and flat-mount skins were prepped. Images of pinned skins were taken within a uniform lighting box with an EIOS2000D camera (Canon) at equal magnification. To quantify stripe width, FIJI (ImageJ) was used to draw line segments spanning each ROI. For each image, ten horizontal lines were measured along the anterior posterior axis of the skin and an average width was calculated. In striped mouse, pigmentation stripes are visible at birth[11] and there are four different regions that can be distinguished and therefore measured: middle stripe, dark stripe 1, light stripe and dark stripe 2. We note that the middle stripe and dark stripe 1 are indistinguishable at midembryonic stages (that is, they are adjacent placode-less regions) but can be distinguished at birth (Fig. 1d). Thus, we refer to them as R1′ and R1′′ to denote that they are derived from embryonic R1. We chose to perform measurements on R1′ and R1′′ because they provide additional data points to test the suggestion that changes in *Sfrp2* lead to differences in stripe width. To measure width of the 'striped area', ten lines were drawn connecting the most ventral boundary of R3 on both sides and averaged. 'Width (% of striped area)' was calculated by dividing the average width of each region (R1, R2, R3 and midline) by the average width of the stripe area. Statistical significance was assessed using two-sided unpaired *t*-tests. Statistical significance was assigned *$P < 0.05$, **$P < 0.01$, ***$P < 0.001$ and ****$P < 0.0001$.

Pigmentation.—To quantify pigment differences, a single image of six *R. pumilio* adults (three *Sfrp2*$^{+/+}$ and three *Sfrp2*$^{-/-}$) was taken within a uniform lighting box with an EIOS2000D camera (Canon). Colour correction was performed on the image using a Pixel Perfect colour checker and Adobe Lightroom software. To quantify pigment differences across animals, a consistently sized ROI was drawn within each stripe region and mean grey value within the ROI was measured using Adobe Photoshop. For R1–R3, mean grey values were measured in three subregions within each stripe region, on each side of the midline (six ROIs total) and averaged. For the midline, mean grey values were measured in five subregions within the midline and averaged. Statistical significance was assessed using two-sided unpaired *t*-tests. Statistical significance was assigned *$P < 0.05$; **$P < 0.01$, ***$P < 0.001$ and ****$P < 0.0001$.

Hair length.—To quantify hair length, individual hair fibres from the different stripes (ten guard hairs per stripe; $n = 3$ animals per genotype) were plucked from preserved skins, placed on a microscope slide and photographed using a stereoscope (Nikon SMZ18). Individual hair was measured using ImageJ. Measurements were taken from the base to the tip of the hair.

Evolutionary analysis

Coding sequence analysis.—Our RER analysis has been previously described[46]. Briefly, we first used RAxML[65] to infer species trees from orthologue sequences of 24 murid genomes. Next, we used the RERConverge v.0.3.0 package[66] to calculate RERs for each sequence in each orthologue alignment. RERConverge generates a consensus tree from various input locus trees (those calculated by RAxML). Each locus tree is then scaled to the consensus tree and residual branch lengths are taken as the RER for each orthologue.

Thus, changes in evolutionary rate are relative to a background expectation based on the class of elements being tested. After calculating RERs for each group of orthologues, highly accelerated sequences were defined as the 95th percentile of genes with a positive RER[46].

The branch-site model was used to test for evidence of positive selection. Briefly, sequence files for *Sfrp2* were first re-aligned using MACSE v.2.06 and branch lengths recalculated with RAxML (v.8.2.12, parameters: -f a -x 12345 -p 12345 -# 100 -m GTRGAMMA). The alignment file was converted to PHYLIP format using msa_view (PHAST v.1.4) and then provided to codeml (PAML v.4.10.0) alongside the gene tree file using a control file. To perform the branch-site test, codeml was run twice, first with the null model (omega fixed, $\omega 2 = 1$) and then with omega being estimated. The difference in ℓ was taken and Chi-square test was performed ($\chi^2_{1,5\%} = 3.84$ (1 degree of freedom at 5% significance))[67,68].

Assay for ATAC-seq.—ATAC-seq was performed on live single-cell suspensions from dorsal skin of E15.5 laboratory mouse 129S2/SvPasCrl ($n = 2$). Tissue was dissected, washed with 1× PBS and incubated in Trypsin (Sigma) at 37 °C for 2 h. The cell suspension was passed through a 40 μm mesh filter and washed with 0.2% BSA/1× PBS. After spinning down the cells for 10 min at 500 r.c.f. (4 °C), the pellet was resuspended in 0.2% 406 BSA/1× PBS, cells were counted and their viability assessed using Trypan Blue (Sigma). Library preparation was carried out with 50,000 live cells using the Omni-ATAC method[69]. Briefly, cells were lysed for 3 min (4 °C) and incubated with TDE1 transposase (Illumina) for 60 min (37 °C). After this, the sample was purified using the Zymo DNA Clean and Concentrator-5 kit (Zymo). Illumina sequencing adaptors and barcodes were added to the transposed DNA fragments by PCR amplification. After examining the purified ATAC-seq libraries on an Agilent Bioanalyzer DNA High Sensitivity chip, we quantified them using a Qubit fluorometer, pooled the libraries and sequenced them in an Illumina NovaSeq 6000 S Prime flowcell as pair-418 end 61 nucleotide reads. Raw ATAC-seq reads were trimmed using 420 NGmerge and mapped to the *M. musculus* reference genome (mm39) using Bowtie. Peak calling on each biological replicate was done using MACS2 (ref. 70) (parameters: --nomodel -q 0.05 --keep-dup all --shift −100 --extsize 200 -g mm --nolambda). Concordance of calls between the two replicates was done using irreproducible discovery rate. Only peaks that passed a false discovery threshold were included in subsequent analyses. BEDTools[71] intersect was then used to remove regions of the ATAC peak calls that directly overlapped with annotated exons, which resulted in a set of genome-wide candidate CREs. We next used Liftoff v.1.6.1 (ref. 72) to lift-over candidate CREs from *M. musculus* to *R. pumilio* and *A. niloticus*. For each of the three species, we used BEDTools closest to search for the candidate CREs that were closest to *Sfrp2*. Our analysis identified the same five candidate CREs for each of the species, indicating a high degree of synteny. These five candidate CREs were aligned using mafft v.7.407 and used for all subsequent analyses.

TF-binding analysis.—Differential motif analysis was carried out using analysis of motif enrichment from MEME suite v.5.5.3 (ref. 73). The *R. pumilio* sequence was tested against the *M. musculus* or *A. niloticulus* used as control sequences. We also conducted the inverse to search for losses that may have occurred in *R. pumilio*. TF motif scans across ATAC peaks were carried out using the find individual motif occurrences (FIMO)[74] program

from the MEME suite. The sequence of each peak for all three species was run using default parameters. For indel analysis, aligned sequences were scanned by eye to identify *R. pumilio*-specific insertions and deletions. These regions, plus 5–10 bp flanking sequences, were then run through FIMO, altering parameters to account for the length of the sequences used (-nmotifs 10 -minw 4 -maxw 30). To identify genes associated to the motifs, Tomtom[75] (MEME suite) was run on motifs that were either uniquely present or absent in *R. pumilio*. These genes were cross-referenced to our whole-dorsum reads per kilobase million counts, which were calculated from the stripe bulk RNA-seq data using the following formula: ((gene raw read)/(total raw read/1,000,000)) × (1,000/gene length).

Reporting summary

Further information on research design is available in the Nature Portfolio Reporting Summary linked to this article.

Data availability

The bulk RNA-seq, scRNA-seq and ATAC-seq reads are submitted under an NCBI BioProject: PRJNA1004353. https://figshare.com/projects/Data_repository_for_A_multifunctional_Wnt_regulator_underlies_the_evolution_of_rodent_stripe_patterns_/175200. Source data are provided with this paper.

Code availability

Code used for scRNA-seq analysis, bulk RNA-seq analysis and comparative genomics is deposited at https://figshare.com/projects/Data_repository_for_A_multifunctional_Wnt_regulator_underlies_the_evolution_of_rodent_stripe_patterns_/175200.

Extended Data

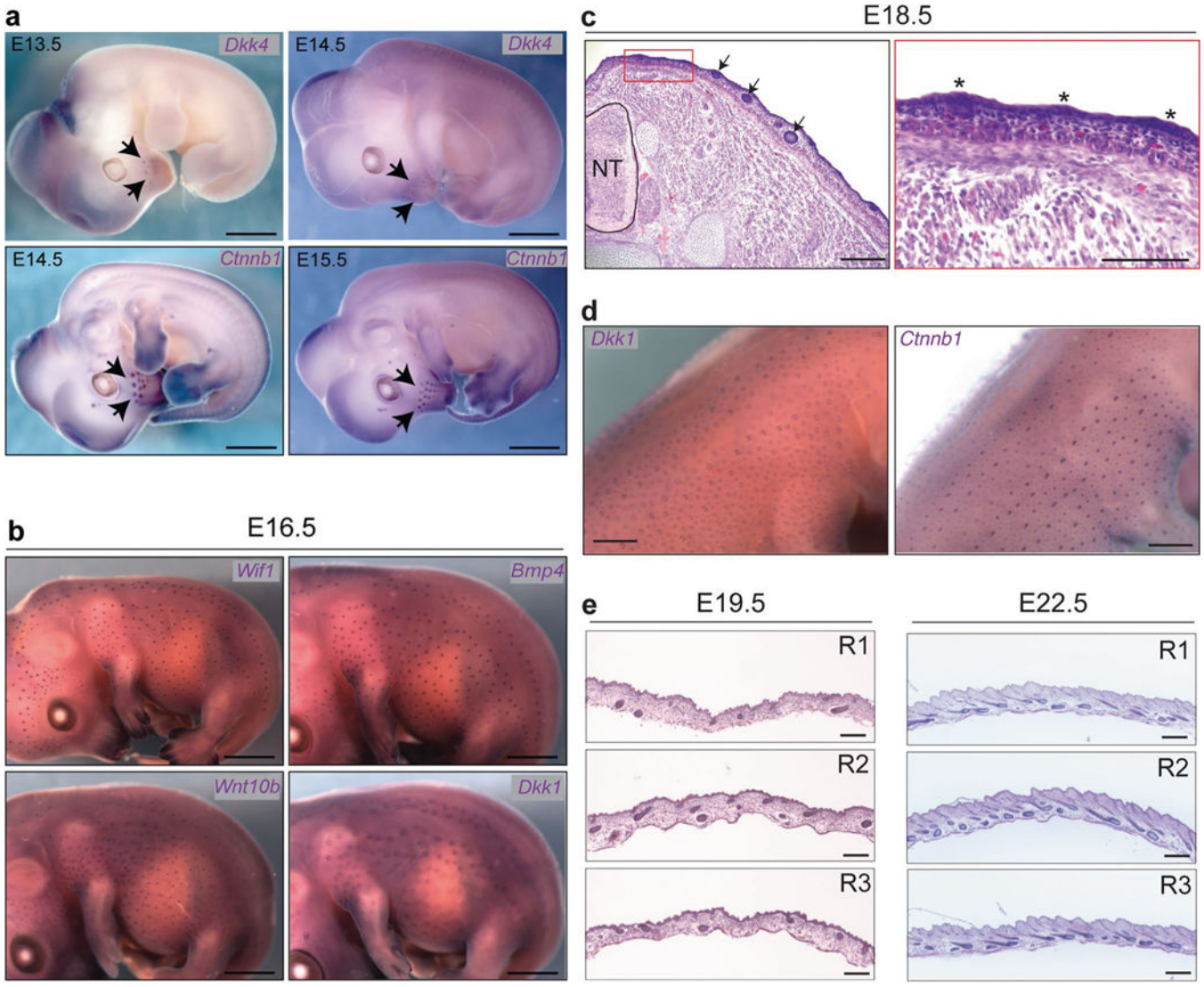

Extended Data Fig. 1 |. Patterns of hair placode formation in striped mice.

a, Side views of E13.5–E15.5 striped mouse embryos showing stages before the emergence of trunk hair placodes. Whole-mount *in situ* hybridization for placode markers *Dkk4* and *Ctnnb1* shows the presence of whisker placodes (arrows), which develop before trunk placodes. No expression is detected in dorsal skin. **b**, Side views of E16.5 striped mouse embryos displaying spatially restricted patterns of trunk hair placode formation, as visualized by whole-mount *in situ* hybridization for placode markers *Wif1*, *Bmp4*, *Wnt10b Dkk1*. **c**, Hematoxylin-Eosin staining on cross-sections of striped mouse E18.5 embryos reveals both mature placodes (arrows) and nascent placodes (asterisks); the latter are evidenced by thickening of the epidermis. **d**, Side views of E18.5 striped mouse embryos showing placode emergence in previously placode-barren regions, as visualized by whole-mount *in situ* hybridization for placode markers *Dkk1* and *Ctnnb1*. **e**, Hematoxilin and Eosin (H&E) stains of longitudinal sections from different dorsal regions in striped mouse

embryos. Placodes in Regions 1 (R1) and 3 (R3) emerge later than those in Region 2 (R2). Scale bars: 5 mm in (**a** and **b**); 200 μm (zoomed out) and 50 μm (inset) in (**c**); 5 mm in (**d**); 100 μm in (**e**). For **a-e**, three individuals per stage per gene were analysed.

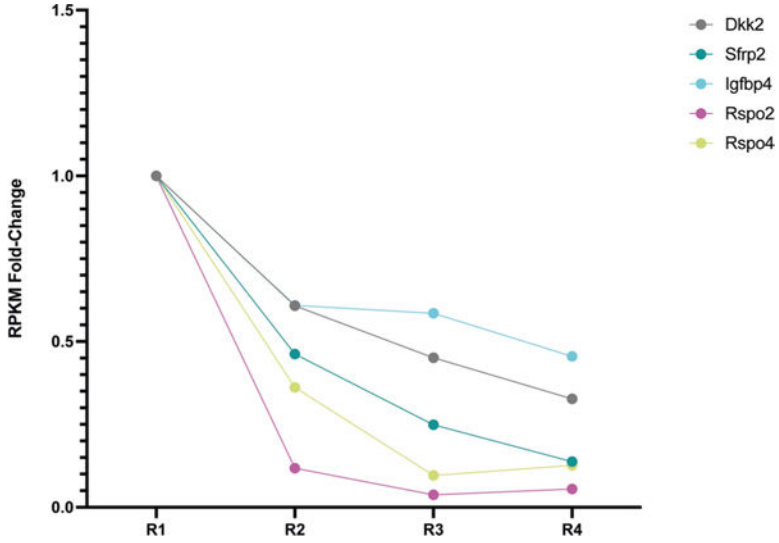

Extended Data Fig. 2 |. Expression of selected Wnt modulators in E16.5 striped mouse embryos. Fold expression changes of Wnt modulators in skin regions (R1, R2, R3, R4) dissected for bulk RNA-seq analysis. Shown are selected modulators that are expressed in a dorsoventral gradient. Fold expression changes were calculated from average FPKM values (n = 3 biologically independent samples.

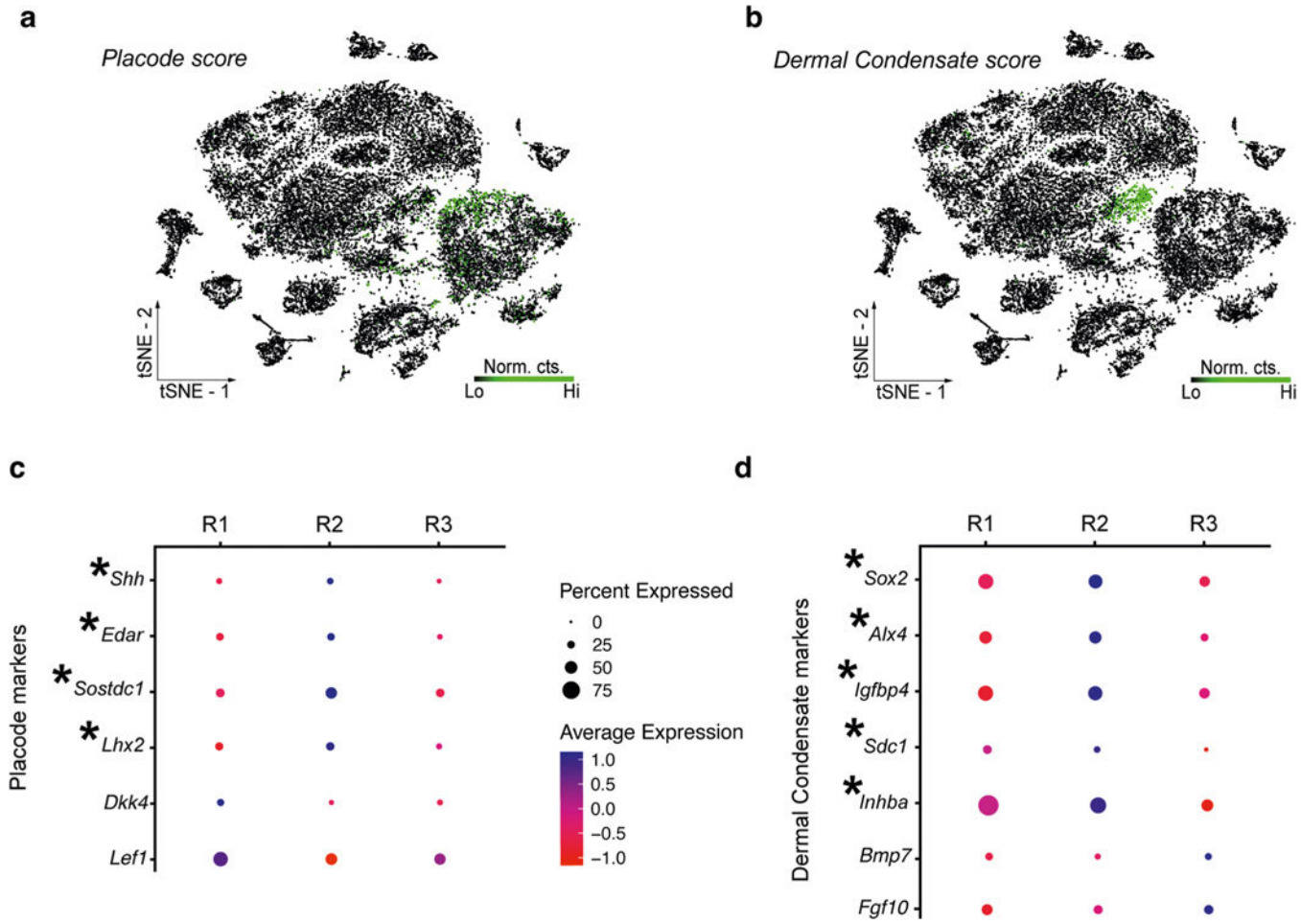

Extended Data Fig. 3 |. Analysis of hair placode and dermal condensate markers.

a-b, Plots showing the subset of cells that express established hair placode (a) and dermal condensate (b) markers in the dorsal skin of E16.5 striped mice. **c-d**, Dot plots of hair placode[25] (c) and dermal condensate[26] (d) markers showing expression changes among the three different dorsal regions sampled. The size of the dot encodes the percentage of cells within a dorsal region, while the colour encodes the average expression level across all cells within a dorsal region (blue is high, red is low). Asterisks depict markers with high expression levels in Region 2 (R2), compared to Region 1 (R1) and Region 3 (R3). As described in the main text, R2 has visible hair follicles at this developmental stage, whereas R1 and R3 do not.

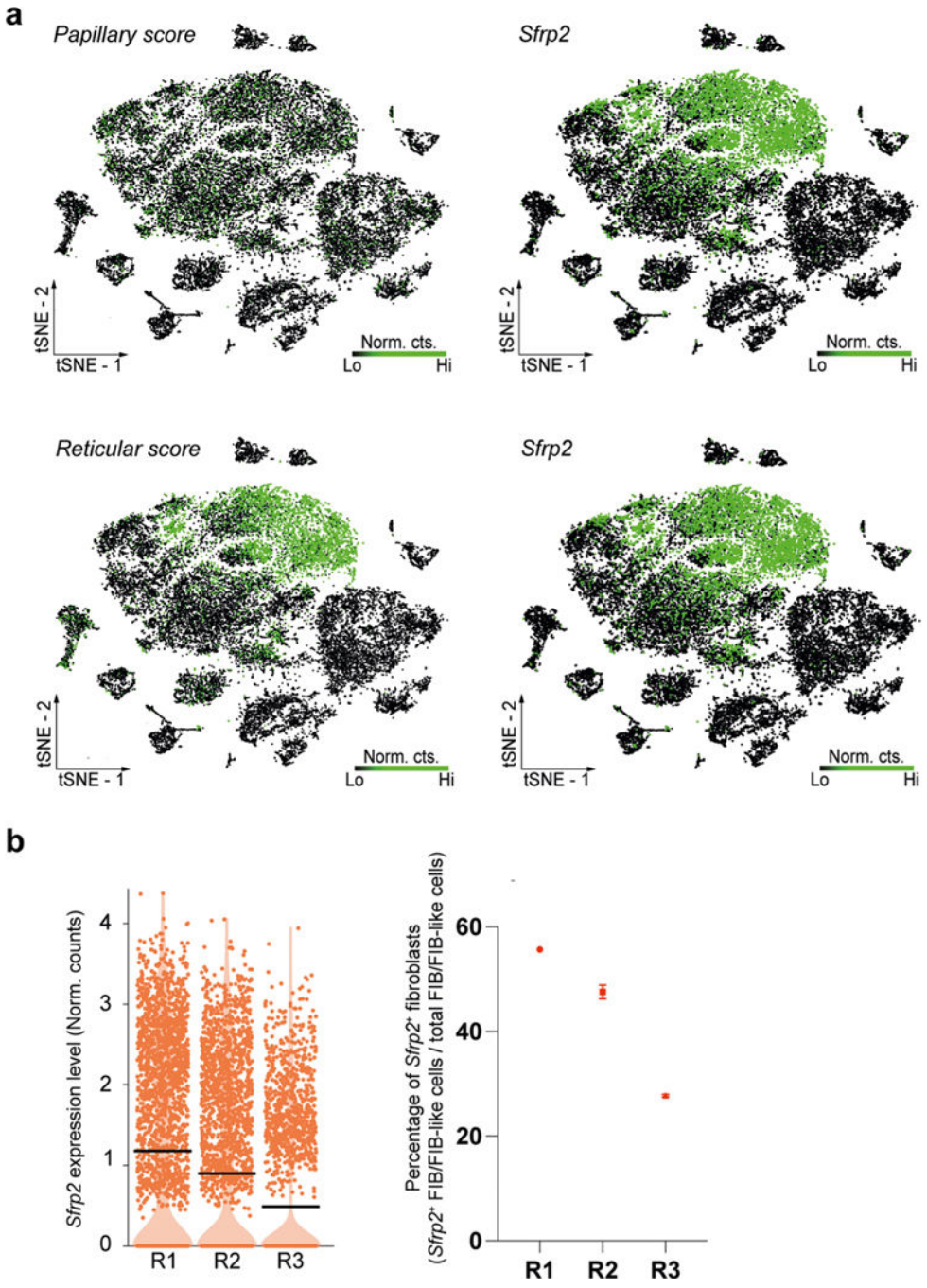

Extended Data Fig. 4 |. Expression of *Sfrp2* in dermal fibroblasts.

a, *Sfrp2* expressing fibroblasts are expressed primarily in the reticular (lower) dermis. Papillary (upper) and reticular (lower) dermis fibroblasts were defined based on previously established markers[3]; Papillary dermis: *Ntn1, Pdpn, Ackr4, Lrig1, Apcdd1;* Reticular dermis: *Tgm2, Cnn1, Cdh2, Mgp, Dlk1*. **b**, At E16.5, expression levels of *Sfrp2* and the percentage of fibroblasts expressing *Sfrp2* are highest in Region 1 (R1) and lowest in Region 3 (R3), in agreement with the dorsoventral gradient revealed by the bulk RNA-seq data. In **b**,

n = 3 biologically independent samples. Left panel: bars represent average expression levels. Right panel: mean values (+/− SEM).

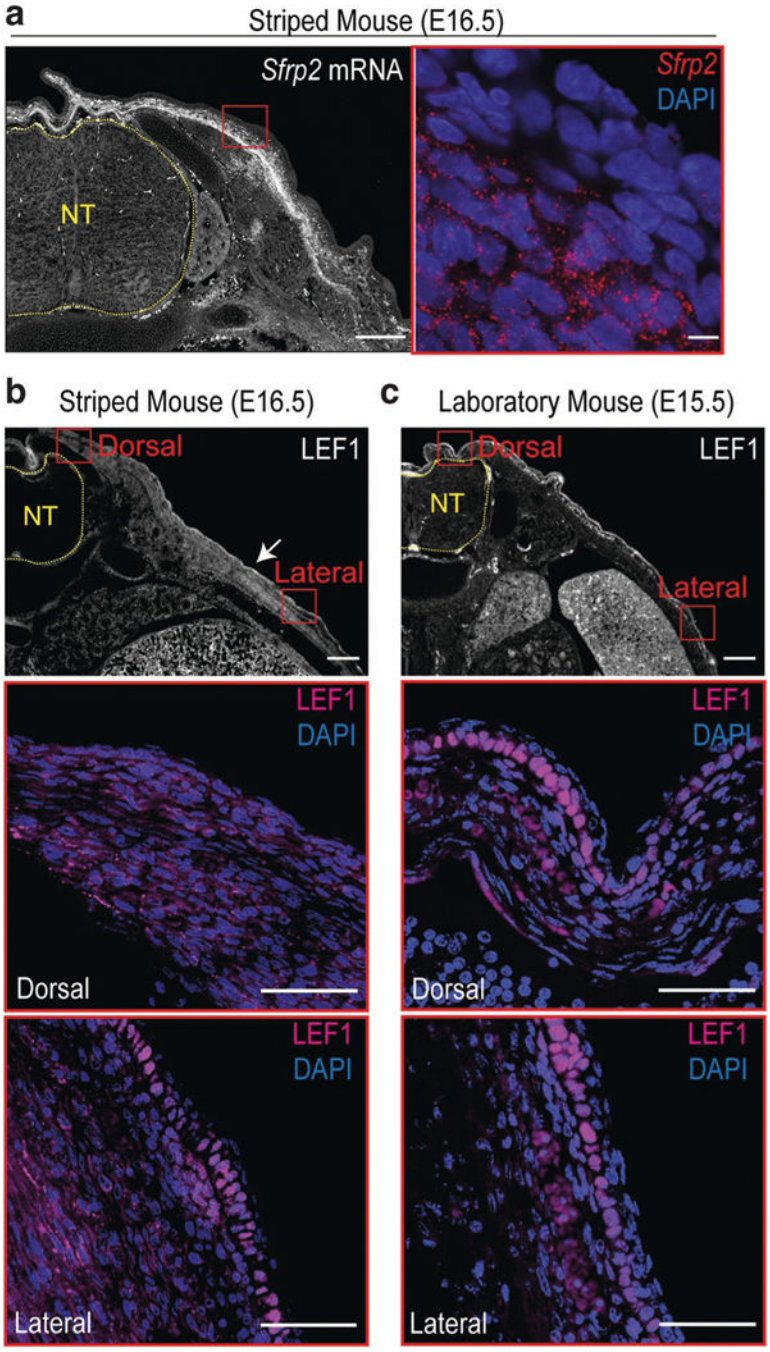

Extended Data Fig. 5 |. High expression of *Sfrp2* in the reticular (lower) dermis coincides with low expression of LEF1.

a, *In situ* hybridization in striped mouse E16.5 embryos shows that *Sfrp2* is primarily expressed in the reticular dermis. Right side image shows expression of *Sfrp2* at subcellular resolution. **b-c**, LEF1 immunostaining in staged matched striped (**b**) and laboratory (**c**) mouse embryos. Red boxes denote zoomed-in regions. Scale bars: 200 μm (zoomed out) and

100 μm (zoomed in) in **a**; 200 μm (zoomed out) and 50 μm (zoomed in) in **b** and **c**. NT = neural tube. For **a-c**, three different individuals were analysed.

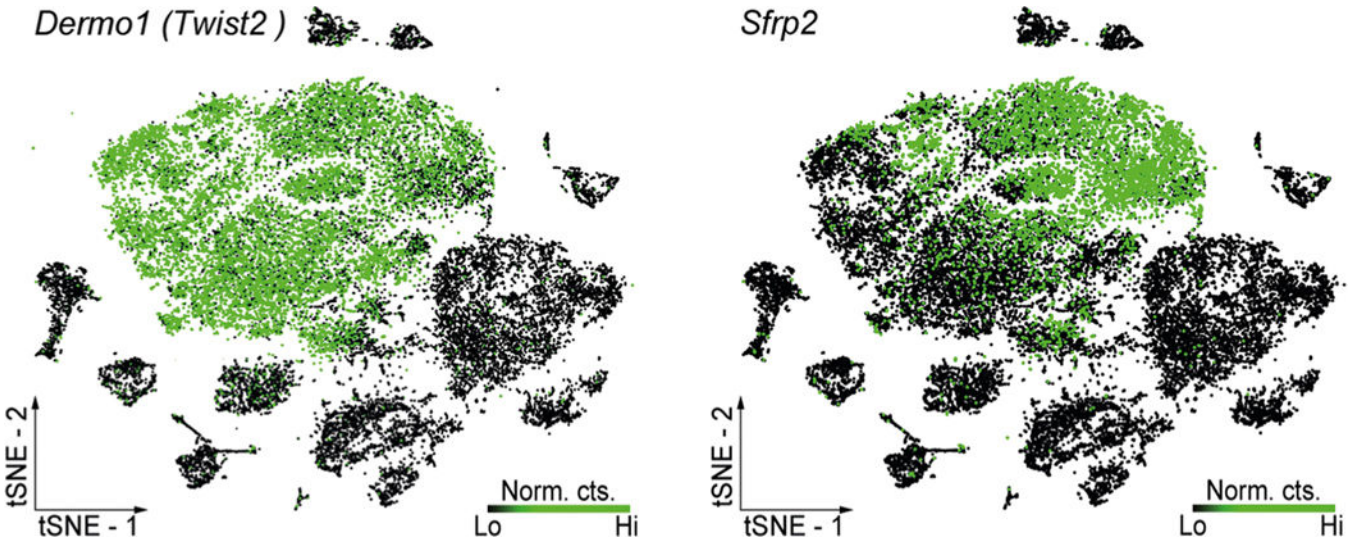

Extended Data Fig. 6 |. *Dermo1* and *Sfrp2* expressing fibroblasts.

A *Dermo-Cre* mouse was used to drive Cre expression in dermal fibroblasts. As illustrated above, a subset of *Dermo1* expressing fibroblasts express *Sfrp2*. Thus, this mouse strain is adequate for driving expression of Cre in cells expressing *Sfrp2*.

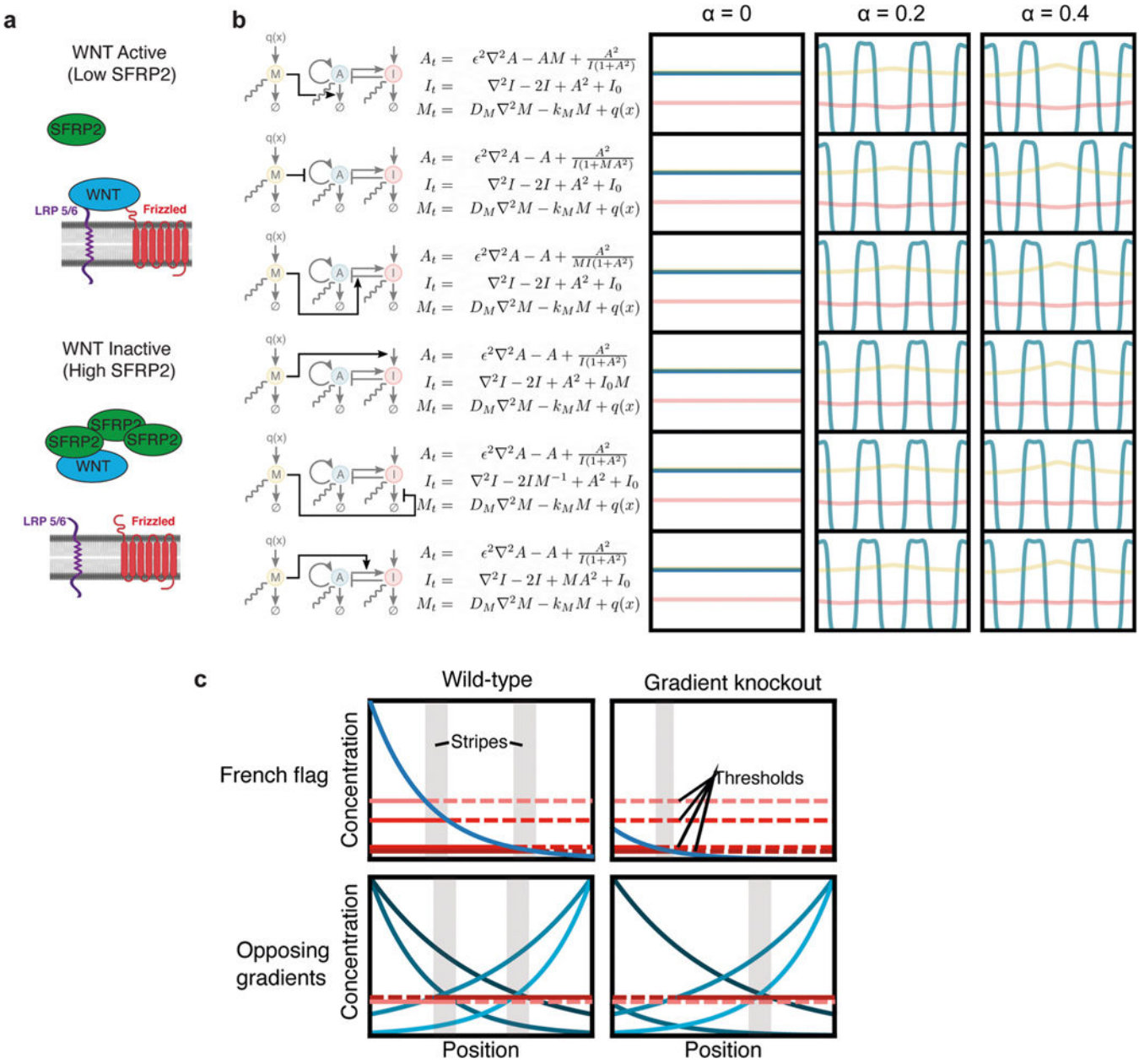

Extended Data Fig. 7 |. Mathematical simulations.

a, Schematic showing the role of *Sfrp2* as an inhibitor of Wnt signalling. **b**, Gradient steepness increases central stripe width independent of model. Each row depicts a schematic and equations governing a particular variant of our modulator-activator-inhibitor system (left) and the resulting simulations of stripe spacing for different gradient steepness values using these models (right). In all cases, gradient steepness affects stripe spacing. **c**, Predictions from an alternative model of positional information. Patterning based on positional information is inconsistent with our experimental results. We illustrate this by considering two standard paradigms for stripe patterning by positional information. Under a classic 'French Flag' model (left, top), each stripe (marked in grey) is assigned to a region of space in which a single morphogen gradient exists between two pathway-

specific threshold concentrations (horizontal red lines). (top, left) Under such a paradigm, a substantial reduction in morphogen expression, in this case by 80 percent, makes it impossible for the gradient to reach certain thresholds entirely, leading to stripe loss. (bottom, left) Alternatively, stripes are frequently determined via an 'opposing gradients' motif via the interaction of multiple gradients. We depict one example, in which each stripe is determined by two opposite facing gradients, such that a stripe forms in the region where each gradient exceeds a morphogen-specific threshold. (right, bottom) Major reduction of a single morphogen eliminates one stripe while leaving the other unperturbed.

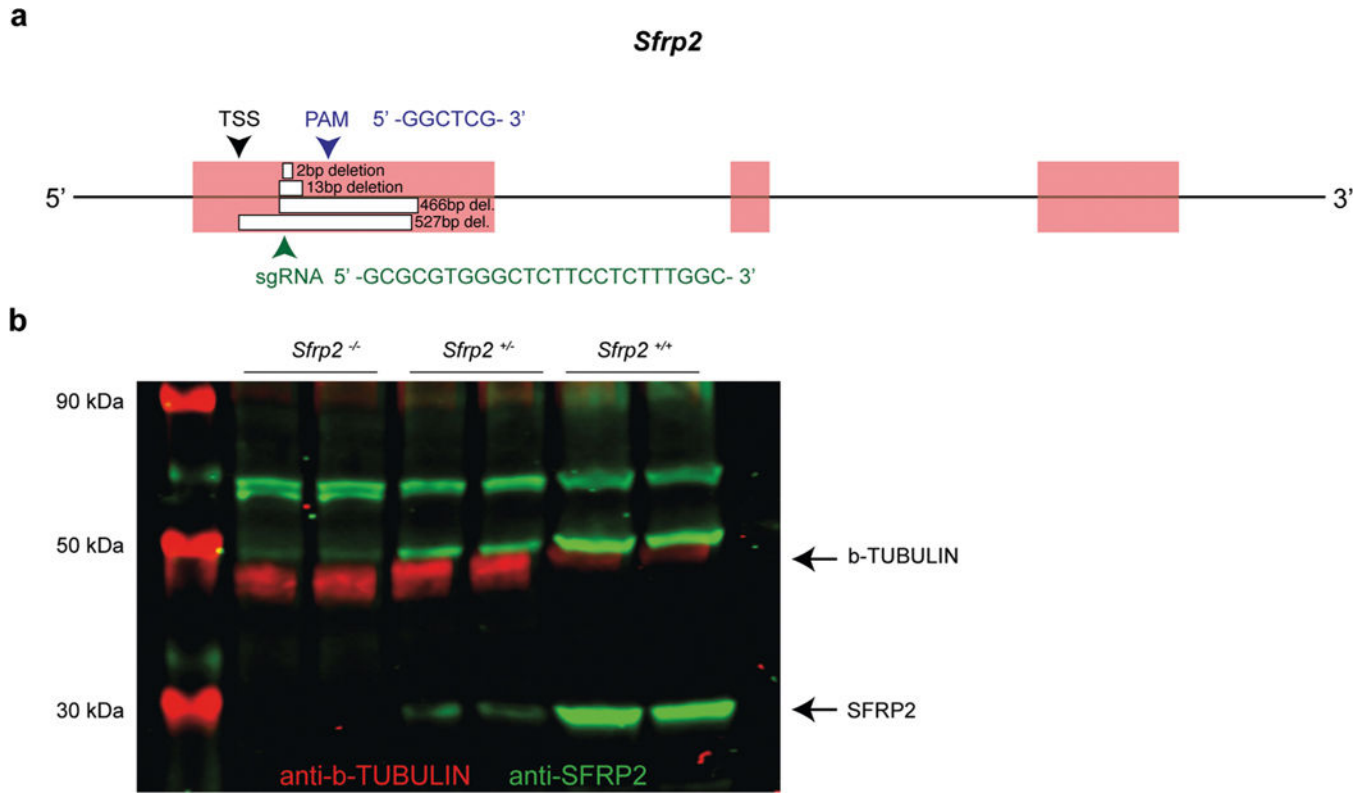

Extended Data Fig. 8 |. Generation of *in vivo* genome editing in striped mouse.
a, Schematic of the *Sfrp2* locus (exons in red) showing the transcriptional start site (TSS), protospacer adjacent motif (PAM) short guide RNA (sgRNA) target/sequence. Four types of deletions were achieved: 2 bp, 13 bp, 466 bp 527 bp (white boxes). All mutations are predicted to cause frameshift mutations. **b**, Representative western blot of individuals carrying different combinations of wild-type and a 13 bp deleted allele (wild type: $Sfrp2^{+/+}$; heterozygous: $Sfrp2^{+/-}$; homozygous: ($Sfrp^{-/-}$). $Sfrp^{-/-}$ have no detectable SFRP2 Protein (green). Bands ~30 kDa correspond to SFRP2 protein. b-TUBULIN (~50 kDa, red) was used as a loading control. In **b**, two different individuals from each genotype were analysed.

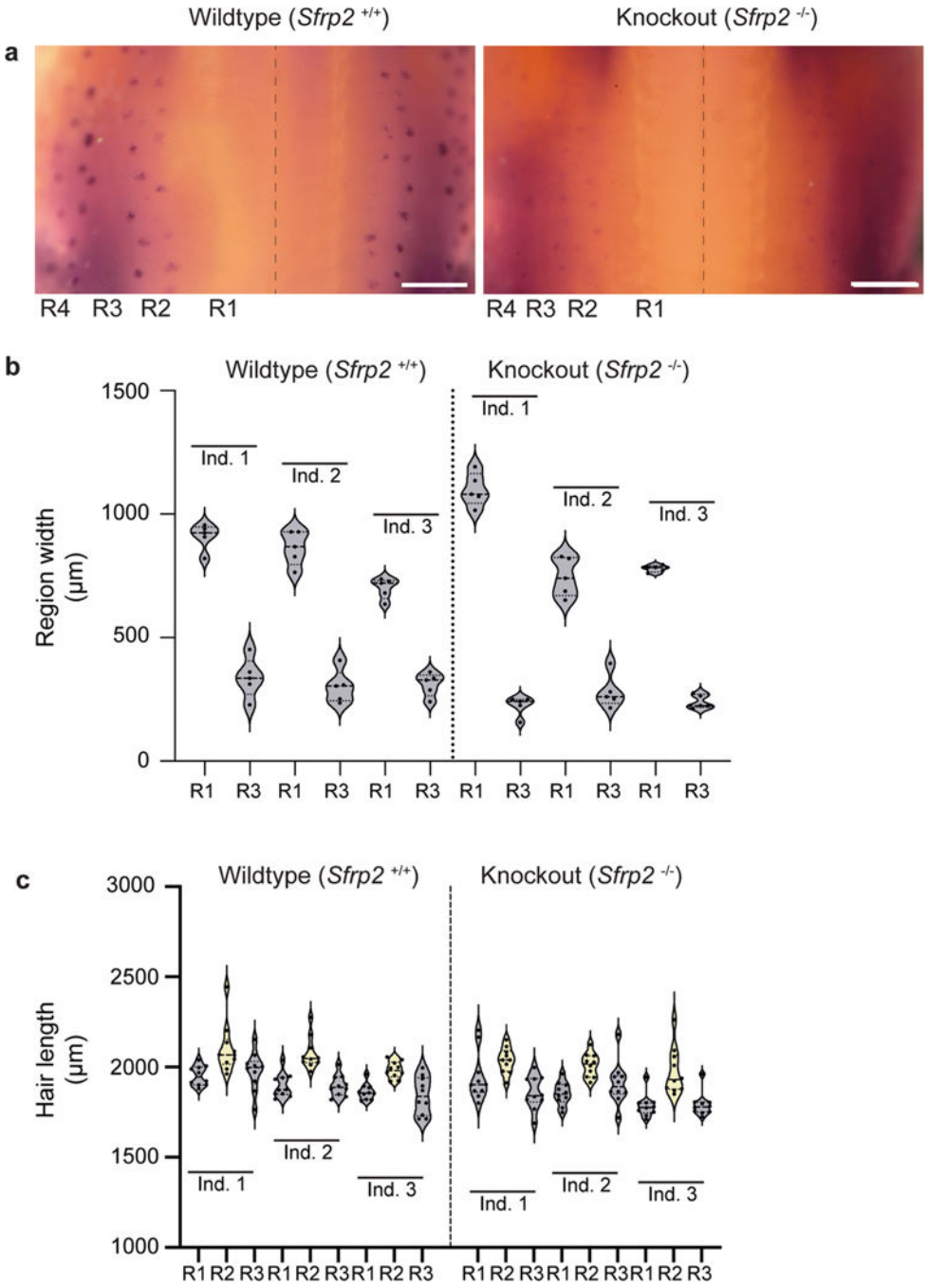

Extended Data Fig. 9 |. Phenotypic characterization of *Sfrp2* mutants.

a and **b**, Whole-mount *in situ* hybridization for *Dkk4* in wild-type and *Sfrp2* knockout E16.5 embryos (**a**) and corresponding width measurements of dorsal regions 1 and 3 (that is, R1 and R3) (**b**). Note that *Dkk4* expression diminishes in response to *Sfrp2* knockout. **c**, Hair length measurements in postnatal day 3 wild-type and *Sfrp2* knockout individuals. In **b** and **c**, n = 3 biologically independent samples for each *Sfrp2* knockout and *Sfrp2* wild-type individuals.

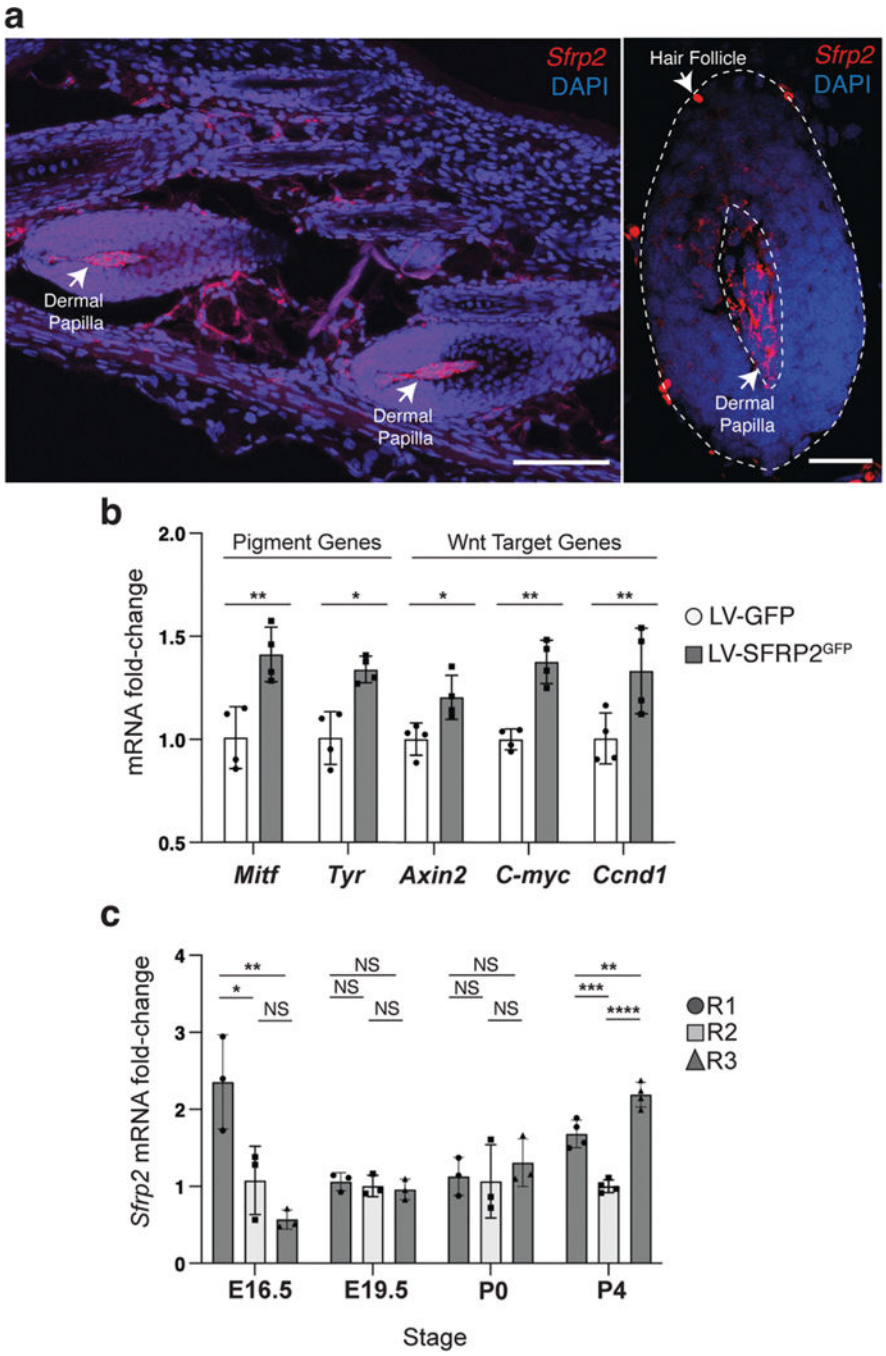

Extended Data Fig. 10 |. *Sfrp2* promotes melanogenesis by activating Wnt signalling.
In situ hybridization showing specific *Sfrp2* expression in the dermal papilla of P4 striped mouse hair follicles. **b**, Melanocytes were stably transduced with either a control (LV-GFP) or an experimental (LV-Sfrp2GFP) lentivirus and expression of Wnt targets and melanogenesis genes in stably transduced control and experimental cells, as determined was determined via qPCR ($P = 0.12026$ (*Axin*); $P = 0.001816$ (*C-myc*); $P = 0.006739$ (*CyclinD*); $P = 0.001040$ (*Mitf*); $P = 0.010712$ (*Tyr*); ANOVA test; N = 4). **c**, Quantitative PCR (qPCR) showing *Sfrp2* mRNA fold change levels along different dorsal skin regions

in embryonic and postnatal stages (E16.5: $P = 0.0283$ (R1vsR2); $P = 0.0062$ (R1vsR3); $P = 0.3959$ (R2vsR3); E19.5: $P = 0.8685$ (R1vsR2); $P = 0.6319$ (R1vsR3); $P = 0.9015$ (R2vsR3); P0: $P = 0.9724$ (R1vsR2); $P = 0.8207$ (R1vsR3); $P = 0.6971$ (R2vsR3); P4: $P = 0.0003$ (R1vsR2); $P = 0.0022$ (R1vsR3); $P = 0.0001$ (R2vsR3); ANOVA test; N = 3 for E16.5, E19.5 P0, N = 4 for P4). Scale bars in **a**: 100 μm (left) and 25 μm (right). In **a**, three different individuals were analysed. In **b** and **c**, data are presented as mean values +/− SEM.

Supplementary Material

Refer to Web version on PubMed Central for supplementary material.

Acknowledgements

We thank members of the Mallarino laboratory; Princeton LAR (C. Dmytrow, K. Gerhart, G. Barnett and J. McGuire) for help with striped mice husbandry; the LSI Genomics Core (W. Wang, J. M. Miller, J. Wiggins and J. Arley Volmar) for help with library preparation and sequencing; the Nikon Center of Excellence Confocal Microscopy Core (S. Wang and G. Laevsky); and members of the Rivera-Perez laboratory (Y. Yoon and J. Gallant) for help with in vivo genome editing experiments. We also thank E. F. Wieschaus, G. Deshpande and P. Holl for insights and discussion. This project was supported by an NIH grant to R.M. (R35GM133758). M.R.J. was supported by an NIH fellowship (F32 GM139253). S.L. was supported by a Presidential Postdoctoral Research fellowship (Princeton University). B.J.B. was supported by an NIH training grant (T32GM007388). C.Y.F. was supported by an NIH fellowship (F32 GM139240-01). C.F.G.-J. is partially supported by UC Irvine Chancellor's ADVANCE Postdoctoral Fellowship Program. Q.N. was partially supported by an NSF grant DMS1763272 and a Simons Foundation grant (594598).

References

1. Mills MG & Patterson LB Not just black and white: pigment pattern development and evolution in vertebrates. Semin. Cell Dev. Biol. 20, 72–81 (2009). [PubMed: 19073271]
2. Caro T. & Mallarino R. Coloration in mammals. Trends Ecol. Evol. 35, 357–366 (2020). [PubMed: 31980234]
3. Cuthill IC et al. The biology of color. Science 357, eaan0221 (2017).
4. Kratochwil CF & Mallarino R. Mechanisms underlying the formation and evolution of vertebrate color patterns. Annu. Rev. Genet. 10.1146/annurev-genet-031423-120918 (2023).
5. Kondo S. & Miura T. Reaction–diffusion model as a framework for understanding biological pattern formation. Science 329, 1616–1620 (2010). [PubMed: 20929839]
6. Kondo S. An updated kernel-based Turing model for studying the mechanisms of biological pattern formation. J. Theor. Biol. 414, 120–127 (2017). [PubMed: 27838459]
7. Turing AM The chemical basis of morphogenesis. 1953. Bull. Math. Biol. 52, 153–197 (1990). [PubMed: 2185858]
8. Vittadello ST, Leyshon T, Schnoerr D. & Stumpf MPH Turing pattern design principles and their robustness. Philos. Trans. A 379, 20200272 (2021).
9. Patterson LB & Parichy DM Zebrafish pigment pattern formation: insights into the development and evolution of adult form. Annu. Rev. Genet. 53, 505–530 (2019). [PubMed: 31509458]
10. Kaelin CB, McGowan KA & Barsh GS Developmental genetics of color pattern establishment in cats. Nat. Commun. 12, 5127 (2021). [PubMed: 34493721]
11. Mallarino R. et al. Developmental mechanisms of stripe patterns in rodents. Nature 539, 518–523 (2016). [PubMed: 27806375]
12. Haupaix N. & Manceau M. The embryonic origin of periodic color patterns. Dev. Biol. 460, 70–76 (2020). [PubMed: 31437441]
13. Kaelin CB et al. Specifying and sustaining pigmentation patterns in domestic and wild cats. Science 337, 1536–1541 (2012). [PubMed: 22997338]
14. Mallarino R, Pillay N, Hoekstra HE & Schradin C. African striped mice. Curr. Biol. 28, R299–R301 (2018). [PubMed: 29614283]

15. Hardy MH The secret life of the hair follicle. Trends Genet. 8, 55–61 (1992). [PubMed: 1566372]
16. Millar SE Molecular mechanisms regulating hair follicle development. J. Invest. Dermatol. 118, 216–225 (2002). [PubMed: 11841536]
17. Andl T, Reddy ST, Gaddapara T. & Millar SE WNT signals are required for the initiation of hair follicle development. Dev. Cell 2, 643–653 (2002). [PubMed: 12015971]
18. van Loon K, Huijbers EJM & Griffioen AW Secreted frizzled-related protein 2: a key player in noncanonical Wnt signaling and tumor angiogenesis. Cancer Metastasis Rev. 40, 191–203 (2021). [PubMed: 33140138]
19. Kim M, Han JH, Kim J-H, Park TJ & Kang HY Secreted frizzled-related protein 2 (sFRP2) functions as a melanogenic stimulator; the role of sFRP2 in UV-induced hyperpigmentary disorders. J. Invest. Dermatol. 136, 236–244 (2016). [PubMed: 26763443]
20. Liang C-J et al. SFRPs are biphasic modulators of Wnt-signaling-elicited cancer stem cell properties beyond extracellular control. Cell Rep. 28, 1511–1525 (2019). [PubMed: 31390565]
21. Lin H. et al. sFRP2 activates Wnt/β-catenin signaling in cardiac fibroblasts: differential roles in cell growth, energy metabolism extracellular matrix remodeling. Am. J. Physiol. Cell Physiol. 311, C710–C719 (2016). [PubMed: 27605451]
22. Gupta K. et al. Single-cell analysis reveals a hair follicle dermal niche molecular differentiation trajectory that begins prior to morphogenesis. Dev. Cell 48, 17–31 (2019). [PubMed: 30595533]
23. Sennett R. et al. An integrated transcriptome atlas of embryonic hair follicle progenitors, their niche, and the developing skin. Dev. Cell 34, 577–591 (2015). [PubMed: 26256211]
24. Rezza A. et al. Signaling networks among stem cell precursors, transit-amplifying progenitors, and their niche in developing hair follicles. Cell Rep. 14, 3001–3018 (2016). [PubMed: 27009580]
25. Sulic A-M et al. Transcriptomic landscape of early hair follicle and epidermal development. Cell Rep. 42, 112643 (2023).
26. Saxena N, Mok K-W & Rendl M. An updated classification of hair follicle morphogenesis. Exp. Dermatol. 28, 332–344 (2019). [PubMed: 30887615]
27. Tsai S-Y et al. Wnt/β-catenin signaling in dermal condensates is required for hair follicle formation. Dev. Biol. 385, 179–188 (2014). [PubMed: 24309208]
28. Gat U, DasGupta R, Degenstein L. & Fuchs E. De Novo hair follicle morphogenesis and hair tumors in mice expressing a truncated beta-catenin in skin. Cell 95, 605–614 (1998). [PubMed: 9845363]
29. Yu K. et al. Conditional inactivation of FGF receptor 2 reveals an essential role for FGF signaling in the regulation of osteoblast function and bone growth. Development 130, 3063–3074 (2003). [PubMed: 12756187]
30. Šošić D, Richardson JA, Yu K, Ornitz DM & Olson EN Twist regulates cytokine gene expression through a negative feedback loop that represses NF-κB activity. Cell 112, 169–180 (2003). [PubMed: 12553906]
31. Hiscock TW & Megason SG Orientation of Turing-like patterns by morphogen gradients and tissue anisotropies. Cell Syst. 1, 408–416 (2015). [PubMed: 26771020]
32. Sick S, Reinker S, Timmer J. & Schlake T. WNT and DKK determine hair follicle spacing through a reaction–diffusion mechanism. Science 314, 1447–1450 (2006). [PubMed: 17082421]
33. Van Gorder RA Pattern formation from spatially heterogeneous reaction–diffusion systems. Philos. Trans. A 379, 20210001 (2021).
34. Gierer A. & Meinhardt H. A theory of biological pattern formation. Kybernetik 12, 30–39 (1972). [PubMed: 4663624]
35. Yochelis A, Tintut Y, Demer LL & Garfinkel A. The formation of labyrinths, spots and stripe patterns in a biochemical approach to cardiovascular calcification. New J. Phys. 10, 055002 (2008).
36. McKay R. & Kolokolnikov T. Stability transitions and dynamics of mesa patterns near the shadow limit of reaction–diffusion systems in one space dimension. Discret. Contin. Dyn. Syst. B 17, 191–220 (2012).
37. Yoon Y. et al. Streamlined ex vivo and in vivo genome editing in mouse embryos using recombinant adeno-associated viruses. Nat. Commun. 9, 412 (2018). [PubMed: 29379011]

38. Iozumi K, Hoganson GE, Pennella R, Everett MA & Fuller BB Role of tyrosinase as the determinant of pigmentation in cultured human melanocytes. J. Invest. Dermatol. 100, 806–811 (1993). [PubMed: 8496620]
39. Edraki A. et al. A compact, high-accuracy Cas9 with a dinucleotide PAM for in vivo genome editing. Mol. Cell 73, 714–726 (2019). [PubMed: 30581144]
40. Enshell-Seijffers D, Lindon C, Wu E, Taketo MM & Morgan BA β-Catenin activity in the dermal papilla of the hair follicle regulates pigment-type switching. Proc. Natl Acad. Sci. USA 107, 21564–21569 (2010).
41. Morgan BA The dermal papilla: an instructive niche for epithelial stem and progenitor cells in development and regeneration of the hair follicle. Cold Spring Harb. Perspect. Med. 4, a015180 (2014).
42. Steingrímsson E, Copeland NG & Jenkins NA Melanocytes and the microphthalmia transcription factor network. Annu. Rev. Genet. 38, 365–411 (2004). [PubMed: 15568981]
43. Jho E-H et al. Wnt/beta-catenin/Tcf signaling induces the transcription of Axin2, a negative regulator of the signaling pathway. Mol. Cell. Biol. 22, 1172–1183 (2002). [PubMed: 11809808]
44. Shtutman M. et al. The cyclin D1 gene is a target of the beta-catenin/LEF-1 pathway. Proc. Natl Acad. Sci. USA 96, 5522–5527 (1999). [PubMed: 10318916]
45. He TC et al. Identification of c-MYC as a target of the APC pathway. Science 281, 1509–1512 (1998). [PubMed: 9727977]
46. Richardson R. et al. The genomic basis of temporal niche evolution in a diurnal rodent. Curr. Biol. 10.1016/j.cub.2023.06.068 (2023).
47. Gao F. et al. EasyCodeML: a visual tool for analysis of selection using CodeML. Ecol. Evol. 9, 3891–3898 (2019). [PubMed: 31015974]
48. Kaelin CB & Barsh GS Genetics of pigmentation in dogs and cats. Annu Rev. Anim. Biosci. 1, 125–156 (2013). [PubMed: 25387014]
49. Keller SH, Jena SG, Yamazaki Y. & Lim B. Regulation of spatiotemporal limits of developmental gene expression via enhancer grammar. Proc. Natl Acad. Sci. USA 117, 15096–15103 (2020).
50. Kaufman MH The Atlas of Mouse Development (Academic Press, 1992).
51. Wu J. & Wang X. Whole-mount in situ hybridization of mouse embryos using DIG-labeled RNA probes. Methods Mol. Biol. 1922, 151–159 (2019). [PubMed: 30838573]
52. Love MI, Huber W. & Anders S. Moderated estimation of fold change and dispersion for RNA-seq data with DESeq2. Genome Biol. 15, 550 (2014). [PubMed: 25516281]
53. Conway JR, Lex A. & Gehlenborg N. UpSetR: an R package for the visualization of intersecting sets and their properties. Bioinformatics 33, 2938–2940 (2017). [PubMed: 28645171]
54. Burns KJ, Vasil GM, Oishi JS, Lecoanet D. & Brown BP Dedalus: a flexible framework for numerical simulations with spectral methods. Phys. Rev. Res. 2, 023068 (2020).
55. Tuckerman LS & Barkley D. in Numerical Methods for Bifurcation Problems and Large-Scale Dynamical Systems (eds Doedel E. & Tuckerman LS.) 453–466 (Springer, 2000).
56. Li H. A statistical framework for SNP calling, mutation discovery, association mapping and population genetical parameter estimation from sequencing data. Bioinformatics 27, 2987–2993 (2011). [PubMed: 21903627]
57. Wolock SL, Lopez R. & Klein AM Scrublet: computational identification of cell doublets in single-cell transcriptomic data. Cell Syst. 8, 281–291 (2019). [PubMed: 30954476]
58. Fan J. et al. Characterizing transcriptional heterogeneity through pathway and gene set overdispersion analysis. Nat. Methods 13, 241–244 (2016). [PubMed: 26780092]
59. Stuart T. et al. Comprehensive integration of single-cell data. Cell 177, 1888–1902 (2019). [PubMed: 31178118]
60. Joost S. et al. The molecular anatomy of mouse skin during hair growth and rest. Cell Stem Cell 26, 441–457 (2020). [PubMed: 32109378]
61. Beronja S, Livshits G, Williams S. & Fuchs E. Rapid functional dissection of genetic networks via tissue-specific transduction and RNAi in mouse embryos. Nat. Med. 16, 821–827 (2010). [PubMed: 20526348]

62. Aasen T. & Izpisúa Belmonte JC Isolation and cultivation of human keratinocytes from skin or plucked hair for the generation of induced pluripotent stem cells. Nat. Protoc. 5, 371–382 (2010). [PubMed: 20134422]

63. Hahn WC et al. Enumeration of the Simian virus 40 early region elements necessary for human cell transformation. Mol. Cell. Biol. 22, 2111–2123 (2002). [PubMed: 11884599]

64. Concordet J-P & Haeussler M. CRISPOR: intuitive guide selection for CRISPR/Cas9 genome editing experiments and screens. Nucleic Acids Res. 46, W242–W245 (2018). [PubMed: 29762716]

65. Stamatakis A. RAxML version 8: a tool for phylogenetic analysis and post-analysis of large phylogenies. Bioinformatics 30, 1312–1313 (2014). [PubMed: 24451623]

66. Kowalczyk A. et al. RERconverge: an R package for associating evolutionary rates with convergent traits. Bioinformatics 35, 4815–4817 (2019). [PubMed: 31192356]

67. Yang Z. PAML: a program package for phylogenetic analysis by maximum likelihood. Comput. Appl. Biosci. 13, 555–556 (1997). [PubMed: 9367129]

68. Álvarez-Carretero S, Kapli P. & Yang Z. Beginner's guide on the use of PAML to detect positive selection. Mol. Biol. Evol. 40, msad041 (2023).

69. Corces MR et al. An improved ATAC-seq protocol reduces background and enables interrogation of frozen tissues. Nat. Methods 14, 959–962 (2017). [PubMed: 28846090]

70. Zhang Y. et al. Model-based analysis of ChIP-seq (MACS). Genome Biol. 9, R137 (2008).

71. Quinlan AR & Hall IM BEDTools: a flexible suite of utilities for comparing genomic features. Bioinformatics 26, 841–842 (2010). [PubMed: 20110278]

72. Shumate A. & Salzberg SL Liftoff: accurate mapping of gene annotations. Bioinformatics 37, 1639–1643 (2021). [PubMed: 33320174]

73. McLeay RC & Bailey TL Motif enrichment analysis: a unified framework and an evaluation on ChIP data. BMC Bioinform. 11, 165 (2010).

74. Grant CE, Bailey TL & Noble WS FIMO: scanning for occurrences of a given motif. Bioinformatics 27, 1017–1018 (2011). [PubMed: 21330290]

75. Gupta S, Stamatoyannopoulos JA, Bailey TL & Noble WS Quantifying similarity between motifs. Genome Biol. 8, R24 (2007). [PubMed: 17324271]

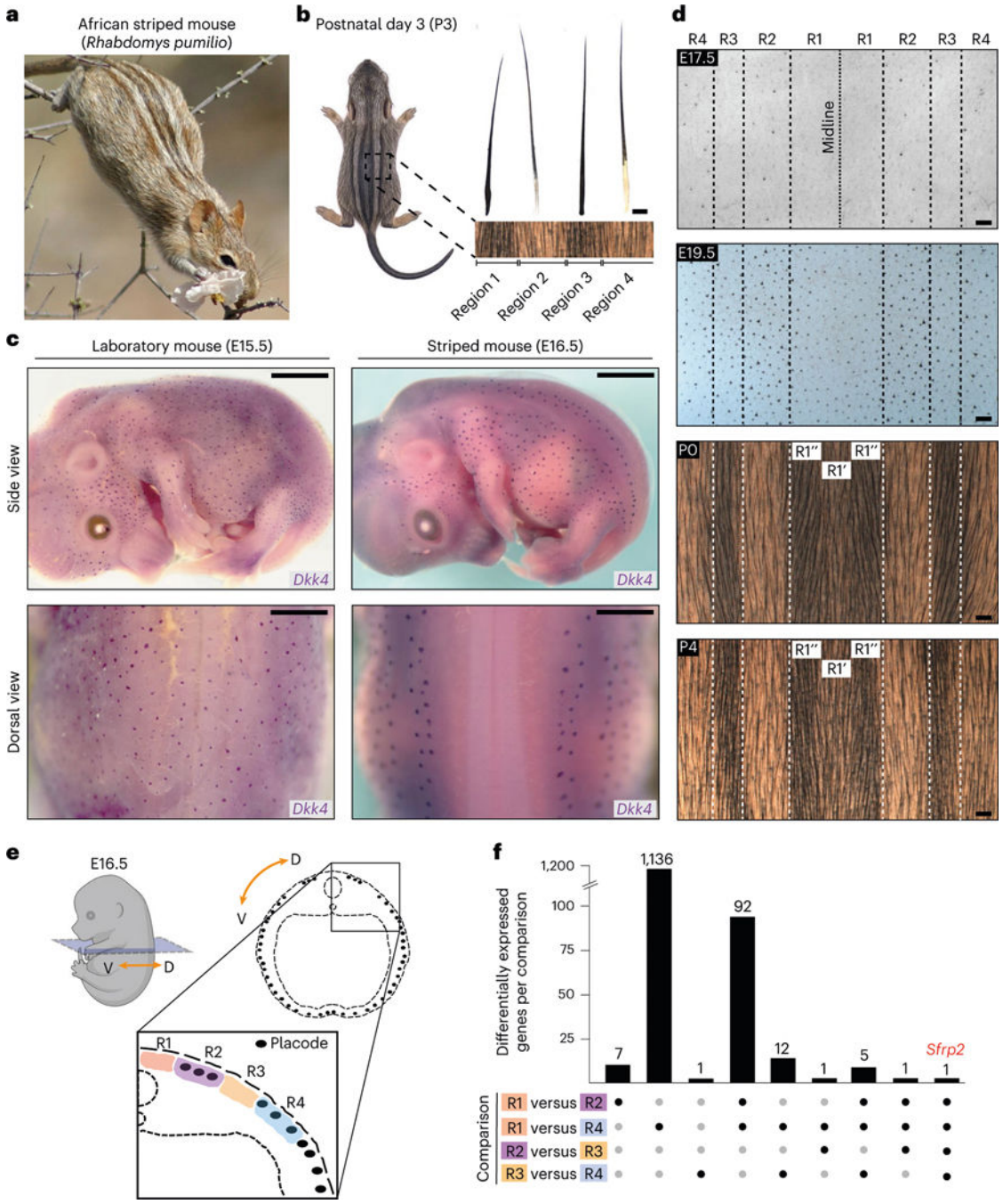

Fig. 1 |. Development of hair placodes and pigment patterns in the African striped mouse.

a, An adult striped mouse in the field. **b**, P3 striped mouse pup displaying the characteristic striped pattern and corresponding differences in hair length across dorsal regions. **c**, Side and dorsal views of E15.5 laboratory mouse and E16.5 striped mouse embryos displaying spatial patterns of hair placode formation, as visualized by whole-mount in situ hybridization for *Dkk4*. **d**, Light-microscopy images of striped mouse flat-mount skins from developmental and postnatal stages (E16.5 to P4) showing how patterns of hair placode development foreshadow pigmentation stripes. R1 encompasses the dorsal-most region in embryos and

is further subdivided into R1′ and R1′′ as the embryo develops. Three samples per stage were analysed. **e**, Schematic of an E16.5 striped mouse embryo displaying regions (R1–R4) dissected for bulk-level RNA-seq analysis. V, ventral; D, dorsal. **f**, UpSet plot summarizing DEGs between R1 and R4. *P* value corrected for multiple testing ($P_{adj} < 0.05$). Each row of dots represents a single pairwise comparison. Black dots indicate there were differentially expressed genes (DEGs) between a given comparison (number of DEGs plotted as columns) whereas grey dots indicate there were not. Scale bars, 5 mm (lateral) and 1 mm (dorsal) in **c**; 100 μm in **d**. Photo credit in **a**: Elaine Kruer. Embryo schematic in **e** created with BioRender.com.

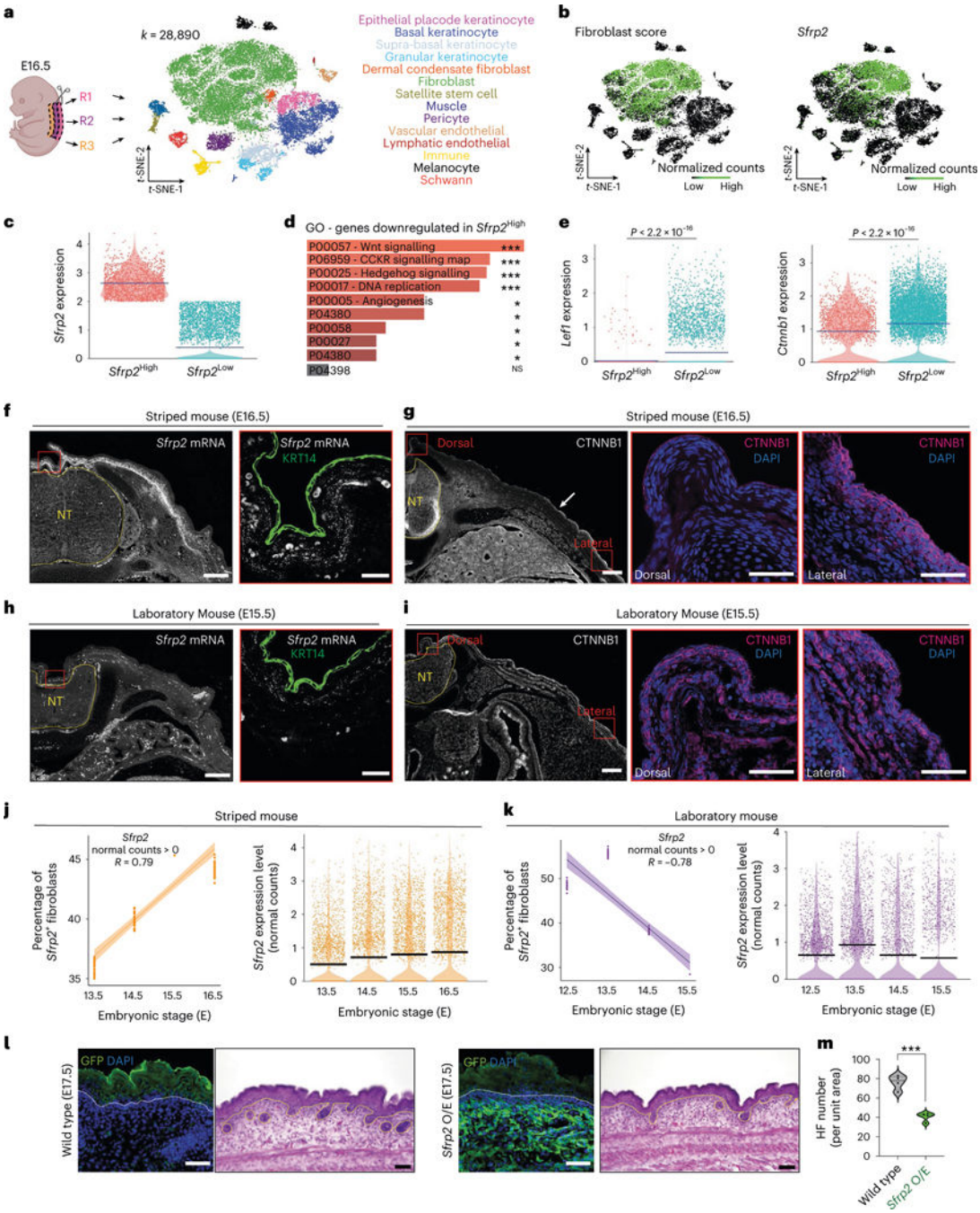

Fig. 2 |. Relationship between *Sfrp2* and Wnt signalling in embryonic skin.

a, Schematic of skin regions (R1–R3) dissected for scRNA-seq (left) and cell-type clustering (right). **b**, Dermal fibroblasts (green, left) cluster with *Sfrp2*-expressing cells (green, right). **c**, Fibroblasts sorted by high (>2 UMI) and low (<2 UMI) *Sfrp2* expression. **d**, Ontology analysis of genes downregulated in *Sfrp2*^{High} cells, show Wnt signalling as the main enriched pathway (*P* values corrected for multiple testing (P_{adj} = 0.00406 (P00057); P_{adj} = 0.0068 (P006959); P_{adj} = 0.0073 (P00025); P_{adj} = 0.0081 (P00017); P_{adj} = 0.0194 (P00005); P_{adj} = 0.0196 (P04380); P_{adj} = 0.0354 (P00058); P_{adj} = 0.04123 (P00027);

P_{adj} = 0.0416 (P04398); P_{adj} = 0.04166 (P04398; one-sided hypergeometric test)). NS, not significant. **e**, *Lef1* and *Ctnnb1* show upregulation in *Sfrp2*^{low} cells ($P = 2.2 \times 10^{-16}$ (*Lef1*); $P = 2.2 \times 10^{-16}$ (*Ctnnb1*); two-sided, non-parametric Wilcoxon rank sum test)). **f**–**i**, In situ hybridization for *Sfrp2* coupled with immunofluorescence (IF) for KRT14 in stage-matched striped mouse (**f**) and laboratory mouse (**h**) embryos. IF for CTNNB1 in stage-matched striped mouse (**g**) and laboratory mouse (**i**) embryos. Red boxes denote zoomed-in regions. At least three samples per stage were analysed in **f**–**i**. **j**,**k**, Comparative scRNA-seq analysis shows both the percentage of fibroblasts that express *Sfrp2* (left, Spearman's correlation, $R = 0.79$) and the expression levels of *Sfrp2* within striped mouse fibroblasts (**j**) increase in the days before visible placode formation while, in laboratory mice (**k**), both the percentage of fibroblasts expressing *Sfrp2* (left, Spearman's correlation, $R = -0.78$) and *Sfrp2* expression levels within those fibroblasts (right) decrease in the days before visible placode formation. **l**,**m**, Representative transverse sections showing that double-transgenic mice have elevated levels of GFP expression (**l**) and lower numbers of hair follicles (**l**,**m**), compared to controls ($P = 0.0002$; two-sided *t*-test; $n = 4$). Panel **l** shows absence of transgene expression in wild type (left) and robust expression of transgene in double-transgenic (*Dermo-Cre*;*Rosa*$^{Sfrp2\text{-}GFP}$) animals (right). Since the vector used contains the *Sfrp2* cDNA cloned in frame with GFP, GFP is a readout of SFRP2 distribution. Bars in **c**, **e**, **j** and **k** represent average expression levels. Scale bars, 200 μm (zoomed out) and 100 μm (zoomed in) **f** and **h**; 200 μm (zoomed out) and 50 μm (zoomed in) in **g** and **i**; and 50 μm in **l**. NT, neural tube. Embryo schematic in **a** created with BioRender.com.

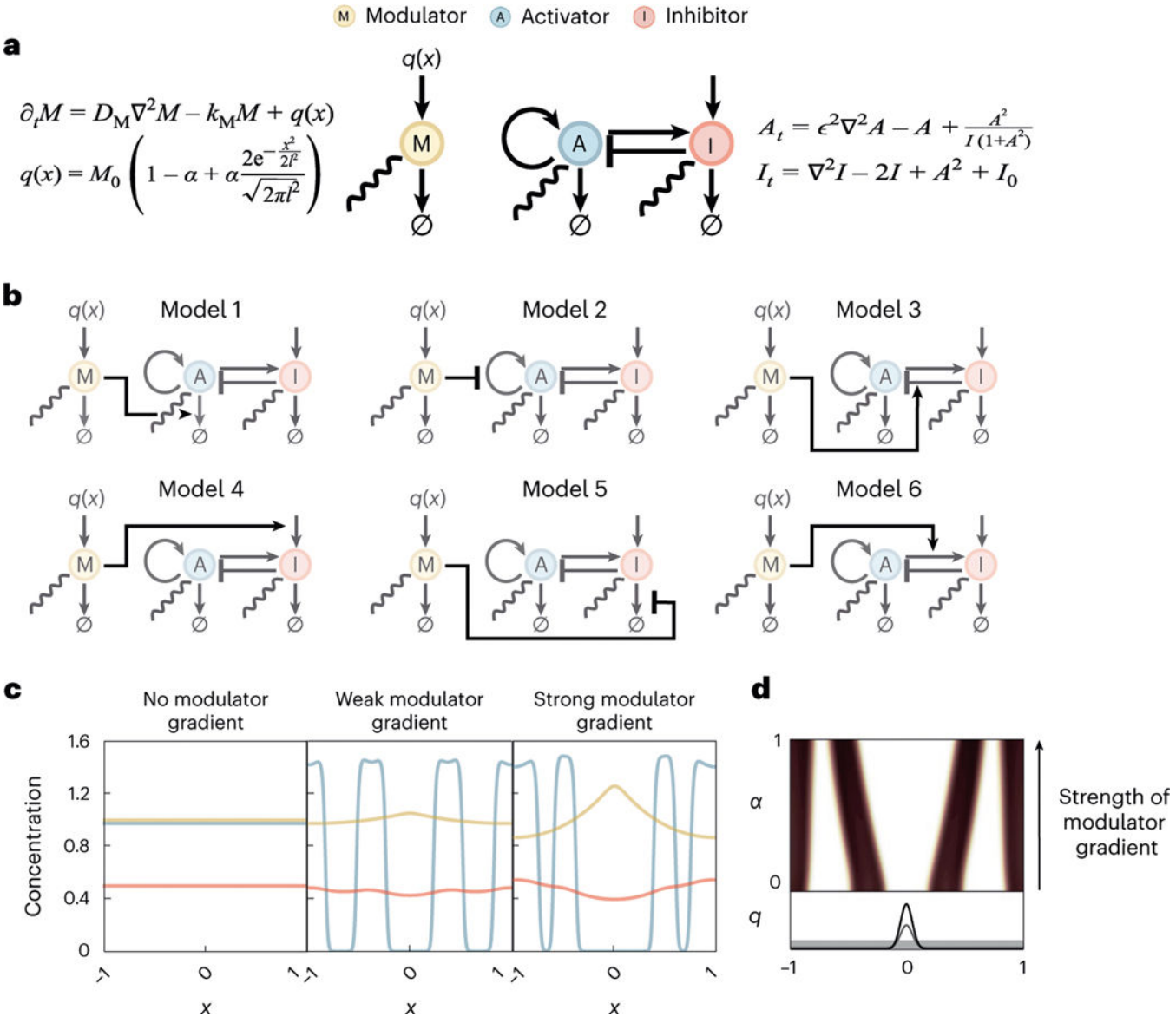

Fig. 3 |. Modulator gradients control stripe patterning in a reaction–diffusion system.

a, We present a two module explanator model for stripe formation. The left module describes a freely diffusible modulator M produced by a non-uniform source term $q(x)$. The non-uniformity of modulator expression is controlled by the gradient steepness parameter α. The right module is a variant of the canonical GM model for Turing pattern formation featuring saturated activator production, which is known to reliably produce stripe patterns. **b**, We consider a range of possible couplings between these two modules, all of which produce qualitatively equivalent results. For further details, see Extended Data Fig. 6. **c**, Example results from model variant 1: (left) In the absence of a modulator gradient, the stripe-less/uniform state is stable. Introduction of modulator gradients destabilize the uniform state and establish stripes (middle, right). **d**, Decreasing α (decreasing the strength of the modulator gradient) corresponds to a narrowing of the medial white region and widening of the lateral white regions (regions corresponding placode-less regions in E16.5

striped mice embryos). This effect is independent of the model choice. Other model choices showed either similar (1–4) or negligible changes (5 and 6) in stripe spacing.

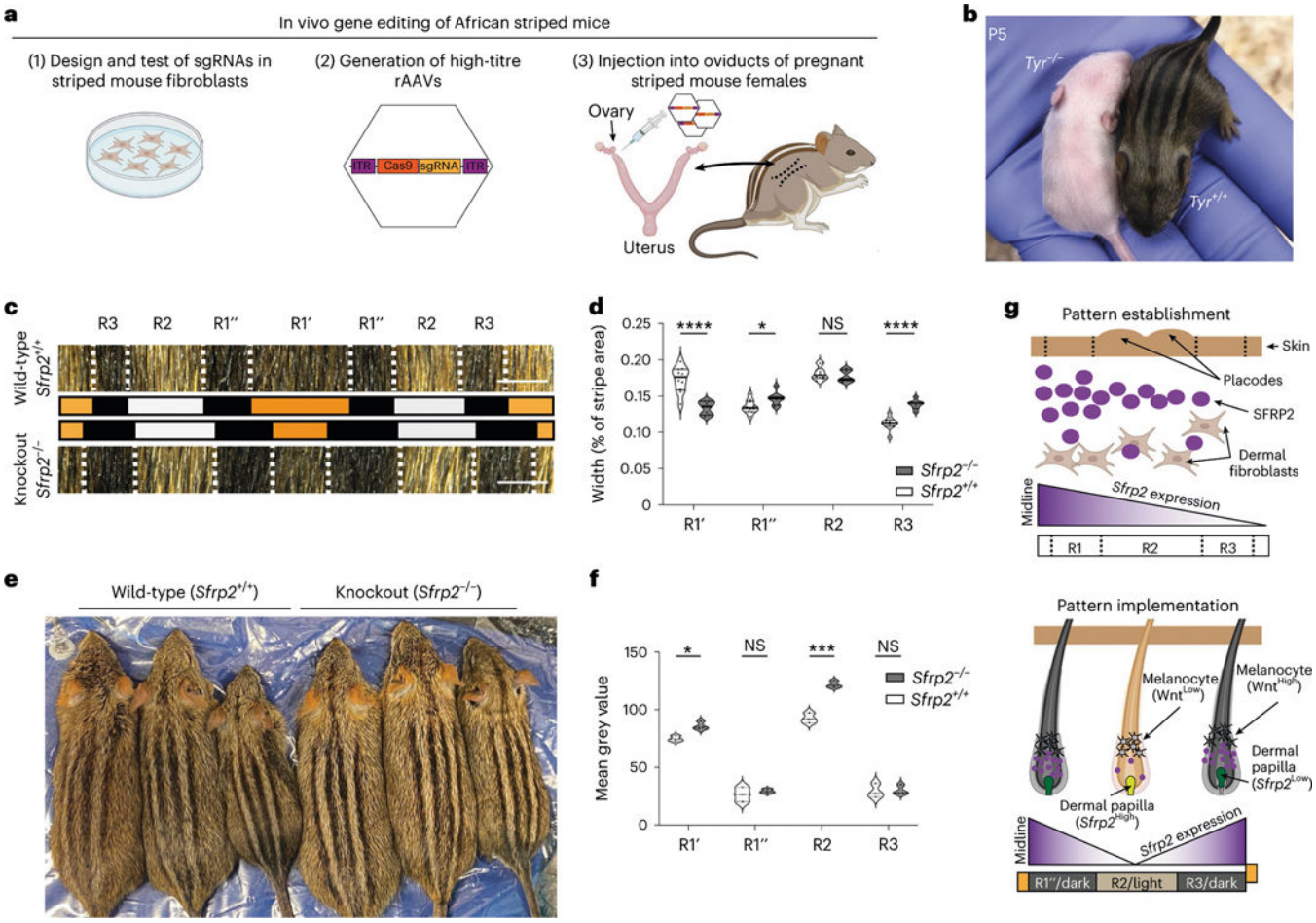

Fig. 4 |. In vivo genome editing reveals that *Sfrp2* regulates striped mouse coat patterns.

a, Schematic of the in vivo gene editing method used. **b**, P5 *Tyrosinase* wild-type ($Tyr^{+/+}$) and knockout ($Tyr^{-/-}$) striped mouse littermates. **c**,**d**, *Sfrp2* regulates stripe pattern width. Shown are representative images (**c**) and measurements (**d**) revealing differences in stripe width between wild-type ($Sfrp2^{+/+}$) and *Sfrp2* knockout ($Sfrp2^{-/-}$) pups ($P = 0.000075$ (R1′), $P = 0.025105$ (R1′′), $P = 0.401739$ (R2), $P = 0.000008$ (R3); ANOVA test; $Sfrp2^{+/+}$; $n = 10$; $Sfrp2^{-/-}$, $n = 7$). **e**, Representative differences in coat colour between $Sfrp2^{+/+}$ and $Sfrp2^{-/-}$ adult mice taken as a single image. **f**, Quantification of pigmentation between $Sfrp2^{+/+}$ and $Sfrp2^{-/-}$ adult mice reveal stripe-specific changes in colour ($P = 0.011884$ (R1′), $P = 0.493389$ (R1′′), $P = 0.000719$ (R2), $P = 0.835735$ (R3); ANOVA test; $Sfrp2^{+/+}$, $n = 3$; $Sfrp2^{-/-}$, $n = 3$). **g**, Model describing the role of *Sfrp2* in establishing (top) and implementing (bottom) the coat pattern in striped mice. Scale bar in **c**, 500 pixels. Schematic in **a** created with BioRender.com.

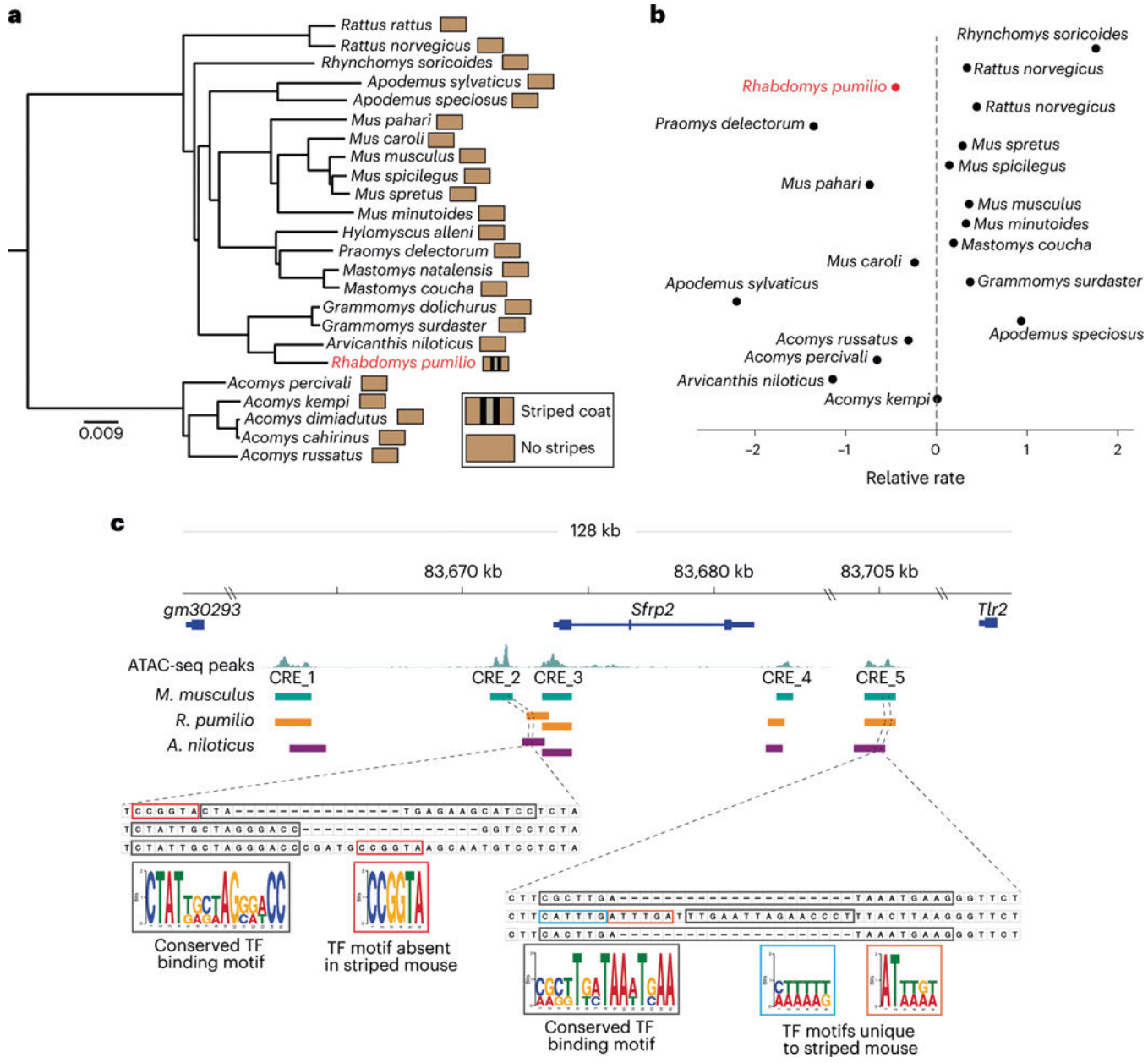

Fig. 5 |. Evolution of the *Sfrp2* locus.

a, Phylogenetic tree of murid species used in our comparative genomic analyses. Phylogeny was redrawn from a previous study[46]. **b**, RERs in different murid species shows that *Sfrp2* does not have an elevated evolutionary rate in the striped mouse (*R. pumilio*; red dot). **c**, The *Sfrp2* locus contains five nearby CREs, whose synteny is conserved in laboratory mouse (*M. musculus*), striped mouse (*R. pumilio*) and African grass rat (*A. niloticus*). Figure illustrates examples of striped mouse-specific deletions and insertions leading to changes in transcription factor (TF) consensus binding motifs. Box colours illustrate whether a TF-binding motif is conserved across all three species or unique to striped mouse.